
This is an electronic reprint of the original article.
This reprint may differ from the original in pagination and typographic detail.

Faradjizadeh, Farzad; Vilathgamuwa, D. Mahinda; Jayathurathnage, Prasad; Ledwich, Gerard

Graph Sets Method (GSM) for Multi-Coil Wireless Power Transfer Systems, Part I: Principles

Published in:
IEEE Transactions on Power Electronics

DOI:
[10.1109/TPEL.2020.2980374](https://doi.org/10.1109/TPEL.2020.2980374)

Published: 01/10/2020

Document Version
Peer-reviewed accepted author manuscript, also known as Final accepted manuscript or Post-print

Please cite the original version:
Faradjizadeh, F., Vilathgamuwa, D. M., Jayathurathnage, P., & Ledwich, G. (2020). Graph Sets Method (GSM) for Multi-Coil Wireless Power Transfer Systems, Part I: Principles. *IEEE Transactions on Power Electronics*, 35(10), 10741-10756. Article 9033999. <https://doi.org/10.1109/TPEL.2020.2980374>

This material is protected by copyright and other intellectual property rights, and duplication or sale of all or part of any of the repository collections is not permitted, except that material may be duplicated by you for your research use or educational purposes in electronic or print form. You must obtain permission for any other use. Electronic or print copies may not be offered, whether for sale or otherwise to anyone who is not an authorised user.

Graph Sets Method (GSM) for Multi-Coil Wireless Power Transfer Systems, Part I: Principles

Farzad Farajizadeh, *Student Member, IEEE*, D. Mahinda Vilathgamuwa, *Fellow, IEEE*, Prasad Jayathurathnage, *Member, IEEE*, and Gerard Ledwich, *Fellow, IEEE*

Abstract—A new approach to derive the equations of Multi-Coil Wireless Power Transfer (MCWPT) systems and to simplify and analyze them is proposed in this paper. By parametrically solving the equations governing MCWPT systems and mapping the resultant transfer functions into Graph Sets (GSs), a set of rules is developed to form the transfer function amongst the voltages across and currents through the coils. Using these rules, some important aspects, such as effective paths for the power to flow, the effect of active coils on each other and on passive coils, dynamic behavior of the system, and reflected impedances can be comprehensively analyzed. This can be done by following GS rules and without complex mathematical calculations. GS Method (GSM) also provides an effective tool to design compensators and power electronic converters driving MCWPT systems and to estimate the receiver (pickup) parameters. Moreover, simplifying the behavior of the coils into three basic types of Current Driven (CD), Voltage Driven (VD), and PaSsive (PS) coils, helps to reduce the complexity of the model and to have a better understanding of the system. This simplification can be further expanded by removing ineffective couplings between the coils. This work is presented in two parts. In Part I, GSM is explained and its different analytical steps are established, and Part II is dedicated to show the effectiveness and validity of this approach by numerically modeling and experimentally evaluating a three-coil MCWPT system.

Index Terms—Graph Sets, Signal Flow Graphs, Wireless Power Transfer.

I. INTRODUCTION

NEAR-FIELD non-radiative Wireless Power Transfer (WPT) systems have been receiving increased attention for a long time. One of the first WPT systems recorded in the history was proposed by Nicola Tesla, in which a pair of loosely coupled coils wirelessly transfer power from one coil to another. The principles of WPT systems have not changed too much since then [1]. These systems exhibit some attractive features, such as the absence of mechanical connectors, safety, charging while the receiver is on the move (dynamic charging), and being eco-friendly in some applications [2]–[4]. These features make them quite useful for charging devices such as laptops, handsets, stationary and moving Electric Vehicles (EVs) [3], [5]–[7].

Scientific progress in studying and designing WPT systems has increased leaps and bounds in recent times as there have

F. Farajizadeh, D. M. Vilathgamuwa, and G. Ledwich are with the Department of Electrical Engineering and Computer Science, Queensland University of Technology, Brisbane, QLD 4001, Australia (e-mail: f.faradjizadeh@gmail.com; mahinda.vilathgamuwa@qut.edu.au; g.ledwich@qut.edu.au).

P. Jayathurathnage is with the Department of Electronics and Nanoengineering, School of Electrical Engineering, Aalto University, Espoo 00076, Finland (e-mail: prasadjayathurathnage@aalto.fi).

been numerous WPT applications in different domains with increasingly complex configurations and diverse specifications. Short range low frequency WPT systems have progressed to medium range with the use of magnetic resonators [8]. Using the same approach, transfer distance has been extended further by using domino repeaters [9], [10]. Multiple transmitters are used to obtain a smoother power profile of the EV dynamic wireless chargers [5], [11]–[14]. Moreover, WPT systems with multiple receivers have been proposed for consumer electronic applications where different receivers are distinct in terms of physical size, power level, and load characteristics [15]. Therefore, WPT systems can encompass multiple transmitters, multiple receivers, and multiple repeaters, or different combinations of these.

Apart from the WPT coil topologies, the configuration of the power source can be either voltage source or current source depending on the application criteria. For example, an LCC compensator along with its input voltage source can function as a current source at its tuning frequency [11], [16]. Likewise, a series compensators helps to achieve ideality of the voltage source at its tuning frequency [17], [18]. With different higher order compensation networks, load independent and/or coupling independent working conditions can also be achieved [19].

From all these examples, it is obvious that the systems are far more complicated than the single-transmitter-single-receiver topology proposed by Nicola Tesla. Increasing the number of coils and energy storage elements (capacitor and inductors) in the compensators significantly increases the system complexity, which makes it extremely difficult to analyze and characterize. Therefore, it is important to investigate a unified analysis to model generalize WPT systems with multiple transmitters, receivers, and passive coils.

To analyze the WPT characteristics, different modeling techniques have been proposed and used. The most fundamental approaches is to use equivalent circuits to model and analyze WPT systems. For this purpose, the coupling between the coils can be modelled in T or Π equivalent circuit, or by a current controlled voltage source. Therefore, using this approach the matrix equations of the system can be mapped to electric circuits. This approach has been extensively used to model and design WPT systems. For example, Rong *et al.* [20] use this technique to analyze meta-material WPT systems, and Fang *et al.* [21] use this concept to optimize WPT coils. The other example is multi-port technique. In this approach, the wireless systems are considered as multi-port systems and the flow of energy is analyzed with the use of network port parameters.

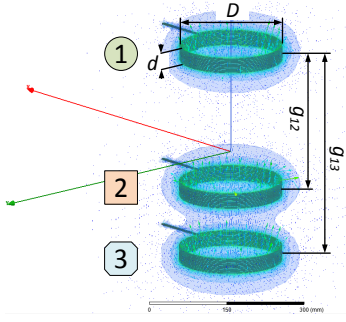


Fig. 1: 3D view of the three-coil prototype.

Coetzee *et al.* [22] use this approach to design a multi-port antenna with isolated ports, he also uses this technique to propose a compact mono-pole array with decoupled ports [23]. The last example is coupled mode theory. In this approach, with the use of differential equations of a WPT system, and re-arranging these equations in terms of energy, the system can be analyzed, optimized and designed. This technique is especially useful for analyzing and designing magnetic resonators [?], [8]. Although these techniques are so useful to understand and analyze WPT systems, when the number of WPT coils increases, the complexity of the resultant circuit makes conventional matrix based equations easier to be dealt with.

In this article, a novel approach of Graph Sets Method (GSM) is introduced to analyze WPT systems consisting of any number of coils. For this purpose coils are categorized into Voltage Driven (VD), Current Driven (CD), and PaSsive (PS) Coils. The proposed GSM is explained with the use of an MCWPT system shown Fig. 1. In this system, coils 1, 2, and 3 depict LCC compensated CD transmitter, series compensated VD transmitter, and PS receiver respectively. Neglecting the Equivalent Series Resistance (ESR), series compensated transmitter can behave as a VD coil [24], and LCC compensated transmitter can behave as a CD coil [16]. Repeater coils can be categorized into VD coils because they are identical in equivalent circuit except for repeaters where the applied voltage V_i is zero (Fig. 2(c)). It should be noted that the proposed GSM can easily be applied to different compensation topologies, and when coils exhibit VD, CD, or PS characteristics, it helps simplifying the approach. The standard state-space equations that govern the system in Fig. 1 consist of 8×8 state matrix that describes the dynamic behavior of the system as characterized by its eigenvalues and eigenvectors. The state-space representation can become even more complicated when the effect of coupling (and its variations) amongst coils over the flow of power is to be studied. Therefore, inspired by Mason's laws to analyze linear systems [25], and other similar works in which signal flow graphs are used to model linear systems [26]–[28], a new approach for formulation of MCWPT equations in a simplistic way is proposed in this article. This approach helps to have a better understanding of the system, in terms of effective power flow paths, finding desirable and undesirable induced voltages and currents, and calculation of the reflected impedances.

The proposed GSM is presented in two parts. In the first part, the principles of this method have been established, and

in Part II, an MCWPT system is numerically analyzed and experimentally tested to show the validity of GSM. Part II also highlights the significance of this approach in different applications. This part (Part I) is organized as follows. To clarify the concept of GSM, WPT coils are categorized into three main types of VD, CD, and PS coils, which are elaborated in Section II along with the equivalent circuit analysis. Then in Section III, how to form the Detailed Model (DM) of an MCWPT system is described, and by parametrically solving the DM of a simple MCWPT system consisting of these different coils, its governing equations are derived to form the graph sets. In this section, it is also explained how different steps of simplifications can reduce the complexity order of the governing equations. Using the mathematical pattern between graph sets, Section IV establishes the basic rules of forming graph sets to represent the system behavior. In Section V, how to derive the gains of voltage path, gains of current path, and reflected impedances from the graph sets is explained. Finally, in Section VI, a summary of how to use the proposed approach in MCWPT systems is explained.

II. ANALYZING AND CATEGORIZING WPT COILS

One of the main purposes of the compensators used in WPT systems is to make WPT coils behave as a voltage source or current source driven coil [29], [30]. Considering this point, coils can be classified into three different types of VD, CD, and PS. In the following subsections, circuit equations are formed and each of these coil types are elaborated.

A. Equivalent Circuit Analysis

In this sub-section, using the equivalent circuit analysis, the governing dynamic equations of a generic WPT system, consisting of CD, VD, and PS coils, as shown in Fig. 1, is systematically formed to show the complexity of the calculations using the conventional standard approach. Kirchoff's laws governing this system in the s-domain provide the following equations.

$$\begin{aligned}
 \begin{bmatrix} E_{L,CD} \\ E_{L,VD} \\ E_{L,PS} \end{bmatrix} &= s \times \underbrace{\begin{bmatrix} L_{CD,CD} & L_{CD,VD} & L_{CD,PS} \\ L_{VD,CD} & L_{VD,VD} & L_{VD,PS} \\ L_{PS,CD} & L_{PS,VD} & L_{PS,PS} \end{bmatrix}}_L \times \begin{bmatrix} I_{L,CD} \\ I_{L,VD} \\ I_{L,PS} \end{bmatrix} = \\
 &= \underbrace{\begin{bmatrix} R_{CD} & O_{CD,VD} & O_{CD,PS} \\ O_{VD,CD} & R_{VD} & O_{VD,PS} \\ O_{PS,CD} & O_{PS,VD} & R_{PS} \end{bmatrix}}_R \times \begin{bmatrix} I_{L,CD} \\ I_{L,VD} \\ I_{L,PS} \end{bmatrix} + \underbrace{\begin{bmatrix} I_{CD,CD} \\ O_{VD,CD} \\ O_{PS,CD} \end{bmatrix}}_{\Lambda_{LP}} \times V_{P,CD} \\
 &= \underbrace{\begin{bmatrix} I_{CD,CD} & O_{CD,VD} & O_{CD,PS} \\ O_{VD,CD} & I_{VD,VD} & O_{VD,PS} \\ O_{PS,CD} & O_{PS,VD} & I_{PS,PS} \end{bmatrix}}_I \times \underbrace{\begin{bmatrix} V_{S,CD} \\ V_{S,VD} \\ V_{S,PS} \end{bmatrix}}_{V_S} + \\
 &= \underbrace{\begin{bmatrix} I_{CD,CD} & O_{CD,VD} \\ O_{VD,CD} & I_{VD,VD} \\ O_{PS,CD} & O_{PS,VD} \end{bmatrix}}_{\Lambda_{LI}} \times \underbrace{\begin{bmatrix} V_{I,CD} \\ V_{I,VD} \end{bmatrix}}_{V_I}
 \end{aligned} \tag{1}$$

$$ES,CD = sL_S I_{L,S,CD} =$$

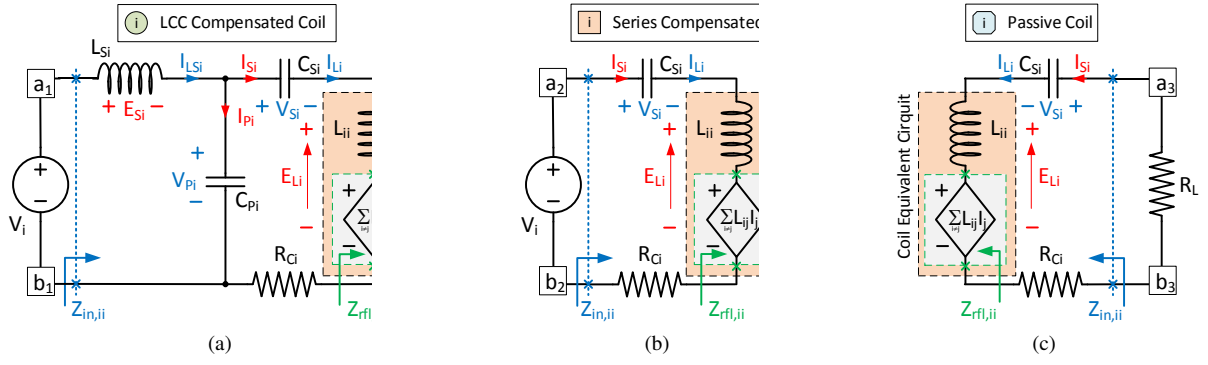


Fig. 2: Equivalent circuit for (a) CD LCC compensated coil 1, (b) VD series compensated coil of 2, and (c) PS compensated coil 3 ($Z_{in,ii}$ is the coil i input impedance seen from the coil terminals, and $Z_{rfi,ii}$ is the reflected impedance due to the other coils seen from coil i terminals).

$$\underbrace{\begin{bmatrix} \mathbf{I}_{CD,CD} & \mathbf{O}_{CD,VD} \\ \mathbf{O}_{CD,VD} & \mathbf{O}_{CD,VD} \end{bmatrix}}_{\mathbf{\Lambda}_{SI}} \times \underbrace{\begin{bmatrix} \mathbf{V}_{I,CD} \\ \mathbf{V}_{I,VD} \end{bmatrix}}_{\mathbf{V}_I} - \mathbf{V}_{P,CD} \quad (2)$$

$$\mathbf{I}_{P,CD} = s\mathbf{C}_P\mathbf{V}_{P,CD} =$$

$$\mathbf{I}_{LS,CD} - \underbrace{\begin{bmatrix} \mathbf{I}_{CD,CD} & \mathbf{O}_{CD,VD} & \mathbf{O}_{CD,PD} \\ \mathbf{O}_{CD,VD} & \mathbf{O}_{CD,VD} & \mathbf{O}_{CD,VD} \\ \mathbf{O}_{CD,PD} & \mathbf{O}_{CD,VD} & \mathbf{O}_{CD,VD} \end{bmatrix}}_{\mathbf{\Lambda}_{PL}} \times \underbrace{\begin{bmatrix} \mathbf{I}_{L,CD} \\ \mathbf{I}_{L,VD} \\ \mathbf{I}_{L,PS} \end{bmatrix}}_{\mathbf{I}_L} \quad (3)$$

$$\underbrace{\begin{bmatrix} \mathbf{I}_{S,CD} \\ \mathbf{I}_{S,VD} \\ \mathbf{I}_{S,PS} \end{bmatrix}}_{\mathbf{I}_S} = \underbrace{\begin{bmatrix} \mathbf{I}_{L,CD} \\ \mathbf{I}_{L,VD} \\ \mathbf{I}_{L,PS} \end{bmatrix}}_{\mathbf{I}_L} =$$

$$s \times \underbrace{\begin{bmatrix} \mathbf{C}_{S,CD} & \mathbf{O}_{CD,VD} & \mathbf{O}_{CD,PS} \\ \mathbf{O}_{VD,CD} & \mathbf{C}_{S,VD} & \mathbf{O}_{VD,PS} \\ \mathbf{O}_{PS,CD} & \mathbf{O}_{PS,VD} & \mathbf{C}_{S,PS} \end{bmatrix}}_{\mathbf{C}_S} \times \underbrace{\begin{bmatrix} \mathbf{V}_{S,CD} \\ \mathbf{V}_{S,VD} \\ \mathbf{V}_{S,PS} \end{bmatrix}}_{\mathbf{V}_S} \quad (4)$$

where \mathbf{I} and \mathbf{O} are the identity and zero matrices respectively, $\mathbf{E}_{L,CD}$, $\mathbf{E}_{L,VD}$, and $\mathbf{E}_{L,PS}$ are the induced voltage vectors in CD, VD and PS coils respectively. $\mathbf{L}_{CD,CD}$, $\mathbf{L}_{CD,VD}$, $\mathbf{L}_{CD,PS} = \mathbf{L}_{PS,CD}$, $\mathbf{L}_{VD,VD}$, $\mathbf{L}_{VD,PS} = \mathbf{L}_{PS,VD}$, and $\mathbf{L}_{PS,PS}$ are the inductance matrices representing the self-inductance and mutual inductance between CD-CD, CD-VD, CD-PS, VD-VD, VD-PS, and PS-PS group of coils. $\mathbf{I}_{L,CD}$, $\mathbf{I}_{L,VD}$, and $\mathbf{I}_{L,PS}$ are the vectors of currents in CD, VD, and PS coils respectively. \mathbf{R}_{CD} , \mathbf{R}_{VD} , and \mathbf{R}_{PS} are the diagonal matrices of the CD, VD, and PS coil resistances respectively. $\mathbf{V}_{S,CD}$, $\mathbf{V}_{S,VD}$, and $\mathbf{V}_{S,PS}$ are the vectors of voltages across series capacitor used in CD, VD, and PS coils respectively. $\mathbf{V}_{I,CD}$ and $\mathbf{V}_{I,VD}$ are the input vectors of voltages driving CD and VD coils, correspondingly. $\mathbf{E}_{S,CD}$ is the vector of induced voltages in the inductances used in the primary loop of the LCC compensators in CD coils. \mathbf{L}_S is the diagonal matrix of the LCC primary loop inductances in the CD coils. $\mathbf{I}_{LS,CD}$ is the vector of currents in the LCC primary loop series inductors seen in CD coils. $\mathbf{V}_{P,CD}$ and $\mathbf{I}_{P,CD}$ are the voltage and current vectors of the LCC parallel capacitors in CD coils respectively. $\mathbf{I}_{S,CD}$, $\mathbf{I}_{S,VD}$, and $\mathbf{I}_{S,PS}$ are the current vectors of the series capacitor used in CD, VD, and

PS coils respectively. $\mathbf{C}_{S,CD}$, $\mathbf{C}_{S,VD}$, and $\mathbf{C}_{S,PS}$ are the diagonal matrices of the series capacitors used in CD, VD and PS coils respectively. Note that the bold variables are used to define matrices throughout this paper. From (1) to (4), the system equation for the three-coil WPT system can be expressed as in equations (5).

$$s \begin{bmatrix} \mathbf{I}_L \\ \mathbf{I}_{LS} \\ \mathbf{V}_{P,CD} \\ \mathbf{V}_S \end{bmatrix} = \begin{bmatrix} \mathbf{L}^{-1}\mathbf{\Lambda}_{LI} \\ \mathbf{L}_S^{-1}\mathbf{\Lambda}_{SI} \\ \mathbf{O} \\ \mathbf{O} \end{bmatrix} \times \mathbf{V}_I + \begin{bmatrix} -\mathbf{L}^{-1}\mathbf{R} & \mathbf{O} & \mathbf{L}^{-1}\mathbf{\Lambda}_{LP} & -\mathbf{L}^{-1} \\ \mathbf{O} & \mathbf{O} & -\mathbf{L}_S^{-1} & \mathbf{O} \\ -\mathbf{C}_P^{-1}\mathbf{\Lambda}_{PL} & \mathbf{C}_P^{-1} & \mathbf{O} & \mathbf{O} \\ \mathbf{C}_S^{-1} & \mathbf{O} & \mathbf{O} & \mathbf{O} \end{bmatrix} \times \begin{bmatrix} \mathbf{I}_L \\ \mathbf{I}_{LS} \\ \mathbf{V}_{P,CD} \\ \mathbf{V}_S \end{bmatrix} \quad (5)$$

The standard MIMO equation of the three-coil prototype is an 8×8 matrix and it provides valuable system information. However, using the standard state-space equation, system properties such as effective power flow path and reflected impedances are not easily achievable, and they demand complex calculations.

B. Voltage Driven Coils

The combination of the input voltage source, the compensator, and the WPT coil that keeps the voltage of the WPT coil constant at its tuned frequency is termed as a *voltage driven* coil. Usually, series compensators serve this function and the simplest way for their modelling is to use the Thevenin Equivalent of the input voltage source and compensator seen from the coil terminals, as shown in Fig. 3. In Fig. 3, L_{ii} and $R_{C,i}$ are the self-inductance and the internal resistance of the coil respectively, and $V_{TH,i}$ and $Z_{TH,i}$ are the Thevenin equivalent voltage and impedance of the source-compensator seen from the coil terminals respectively. Based on the Thevenin equivalent circuit shown in Fig. 3, the governing equation of this coil can be written as follows:

$$V_{TH,i} = \underbrace{(Z_i + Z_{TH,i})}_{Z_{ii}} I_i + E_i \Rightarrow V_{TH,i} = Z_{ii} I_i + \sum_{i \neq j}^n L_{ij} s I_j \quad (6)$$

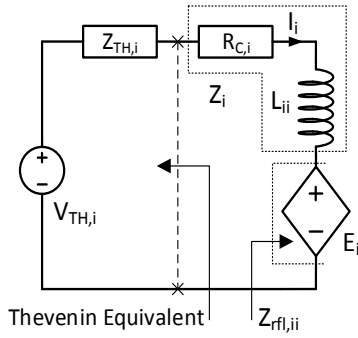


Fig. 3: Thevenin equivalent of the source-compensator set to drive a WPT coil.

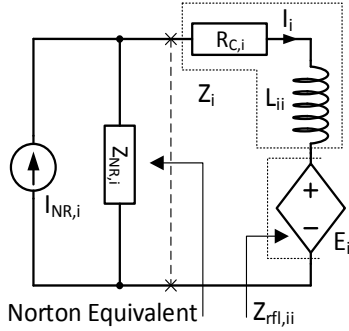


Fig. 4: Norton equivalent of the source-compensator set to drive a WPT coil.

where Z_{ii} is the coil overall impedance, I_i is the coil current, E_i is the induced voltage in the i^{th} coil, n is the total number of coils in an MSWPT system, and L_{ij} is the mutual inductance between coils i and j .

This model represents a realistic behavior of a VD coil. Therefore, it can be used to model the dynamic behavior of the system. To achieve ideal behavior of a voltage driven coil, E_i must be equal to $V_{TH,i}$, which means $Z_{ii} \rightarrow 0$. However, due to the presence of series equivalent resistor in the voltage source, compensator, and the coil, this ideal behavior cannot be fully realized. To obtain a near-ideal VD functionality, the quality factor of the compensator should be kept high. Based on this definition, repeaters can be considered as VD coils with V_{TH} equal to zero.

C. Current Driven Coils

Next, the current driven coils are described. This type of coil is driven by a current source, which can be made by the combination of a voltage source and an LCC compensator [11], [12], [16]. To have a realistic representation, Norton equivalent of a current source with the parallel impedance of $Z_{NR,i}$ is employed to model the LCC compensated CD coil as shown in Fig. 4. The governing equation of this system is written as

$$I_i = \frac{Z_{NR,i}}{Z_{NR,i} + Z_i} I_{NR,i} - \frac{1}{\underbrace{Z_{NR,i} + Z_i}_{Z_{ii}}} E_i \Rightarrow$$

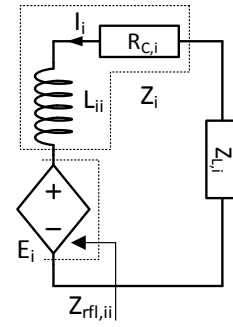


Fig. 5: Equivalent circuit diagram of a passive coil connected to the load $Z_{L,i}$.

$$I_i = \frac{Z_{NR,i}}{Z_{ii}} I_{NR,i} - \frac{1}{Z_{ii}} \sum_{i \neq j}^n L_{ij} s I_j \quad (7)$$

where $I_{NR,i}$ and $Z_{NR,i}$ are the Norton equivalent current and impedance of the source-compensator combination seen from the coil terminals respectively. For an ideal CD coil, $I_{NR,i}$ is equal to I_i ; this occurs when $Z_{NR,i} \rightarrow \infty$. Unlike VD coils, the ideal behavior of a CD coil is more easily attainable in a practical implementation. It is worthy to mention that for both CD and VD coils, Norton to Thevenin conversion (or vice versa) can be done.

D. Passive Coils

PS coils are not driven by any power supply. They receive energy from the other active coils through the couplings. The topology of PS coil can be modelled as shown in Fig. 5. The governing equation of a PS coil is as follows:

$$I_i = \frac{E_i}{Z_{L,i} + Z_i} \Rightarrow I_i = \frac{1}{\underbrace{Z_{L,i} + Z_i}_{Z_{ii}}} \sum_{i \neq j}^n L_{ij} s I_j \quad (8)$$

In this equation, $Z_{L,i}$ includes the impedance of the load and the compensator seen from the coil terminals, the compensator can be either series, parallel, or any other type [12], [31]. Worthy to mention that, repeaters can also be considered as PS coils, but as ideally there is no energy consuming elements in these coils, and they behave similar to VD coils (when $V_{TH=0}$), they are categorized in VD type.

Considering the equations governing these three types of coils, there are some general rules upon which the power flow paths in MCWPT systems can be analyzed. These rules can be found by sorting the governing equations of the system as explained in equations (6) to (8), and solving the resultant equations based on the independent variables ($I_{NR,i}$ and $V_{TH,i}$) and dependent coil electric variables (I_i and E_i).

III. MODELING MCWPT SYSTEMS WITH THE USE OF GRAPH SETS METHOD (GSM)

In this section, the proposed GSM for an MCWPT system is explained. To this end, the dependent variables (induced voltage E_i and current I_i of each coil) are meant to be calculated based on the independent electric variables (the current source $I_{NR,i}$ and the voltage source $V_{TH,i}$). Then the gains

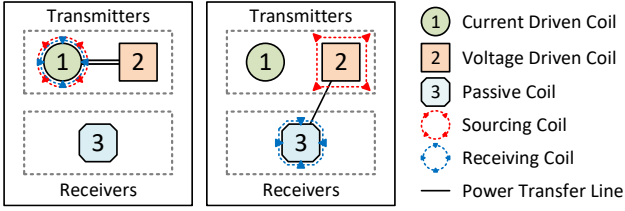


Fig. 6: Symbols used to represent three different coils in a three-coil MCWPT system and to show graph sets, as lines, sourcing coils (as red outward-arranged symbols), and sinking coils (as blue inward-arranged symbols).

linking the dependent variables to the independent variables are analyzed. All the gains have the same denominator but different numerators. Some graph sets are formed depending on how the sub-terms of denominator and numerator link overall impedances (Z_{ii}) thorough the mutual inductances (L_{ij}). Each graph set describes a denominator or a numerator in a linking gain, and each graph in a graph set defines a sub-term in that denominator or numerator.

The graphs contain some nodes and lines. Nodes represent the overall impedance of each coil (Z_{ii}), and based on the coil type, different symbols are used to represent them, as shown in Fig. 6. In addition, lines are used to describe the mutual inductance between different coils involved in the flow of power, as shown in Fig. 6.

To represent the system with the use of GSM, the system is analyzed when one coil is activated at a time (termed as *sourcing coil* as represented by outward arrows in Fig. 6), and how it affects a set of coils, including itself, through the couplings is investigated. The inward-arranged symbols in Fig. 6 (b) stand for a specific sinking coil which is under consideration. Between each sourcing and sinking coil, there can be different possible ways to transfer power through a set of graphs as shown by the lines in Fig. 6, and all these graph sets collectively characterize the complete WPT system. Paths including two coils and starting from one coil and ending up at the same coil is represented by a double-line.

To start the analysis, the detailed model (DM) of the system is introduced first, and then, by converting the realistic Norton equivalent of the CD coil to ideal, the first step of approximation (AP1) is carried out. Then, in the second stage of approximation (AP2), the ideal models of both CD and VD coils are used to obtain the graph sets and their corresponding gains. Finally, the effect of negligible mutual inductances are omitted in the third stage of approximation AP3. Comprehensive explanations on DM, AP1, AP2, and AP3 are presented in the subsequent sections.

A. Detailed Model (DM) of an MCWPT

In general, for an MCWPT system consisting of m coils, which are n_1 CD coils, n_2 VD coils, and n_3 PS coils, the matrix equation linking dependent to independent variables can be written as follows:

$$\underbrace{\begin{bmatrix} \mathbf{E} \\ \mathbf{I} \end{bmatrix}}_{\text{Dependent Variables}} = \underbrace{\begin{bmatrix} \hat{\mathbf{G}}_{\mathbf{V}\mathbf{V}} & \mathbf{G}_{\mathbf{I}\mathbf{V}} \\ \mathbf{G}_{\mathbf{V}\mathbf{I}} & \hat{\mathbf{G}}_{\mathbf{I}\mathbf{I}} \end{bmatrix}}_{\text{Gains}} \times \underbrace{\begin{bmatrix} \mathbf{V}_{\mathbf{TH}} \\ \mathbf{I}_{\mathbf{NR}} \end{bmatrix}}_{\text{Independent Variables}} \quad (9)$$

where $[\mathbf{I}_{\mathbf{NR}}]_{n_1 \times 1}$ is the vector of CD coil Norton currents, $[\mathbf{V}_{\mathbf{TH}}]_{n_2 \times 1}$ is the vector of VD coil Thevenin voltages, $[\mathbf{E}]_{m \times 1}$ is the vector of induced voltages in the coils, and $[\mathbf{I}]_{m \times 1}$ is the vector of induced currents in the coils, $[\hat{\mathbf{G}}_{\mathbf{V}\mathbf{V}}]_{m \times n_2}$ is the dimensionless matrix of gains between \mathbf{E} and $\mathbf{V}_{\mathbf{TH}}$, $[\mathbf{G}_{\mathbf{I}\mathbf{V}}]_{m \times n_1}$ is the matrix of gains between \mathbf{E} and $\mathbf{I}_{\mathbf{NR}}$ (in Ω), $[\hat{\mathbf{G}}_{\mathbf{V}\mathbf{I}}]_{m \times n_2}$ is the matrix of gains between \mathbf{I} and $\mathbf{V}_{\mathbf{TH}}$ (in Ω^{-1}), and $[\hat{\mathbf{G}}_{\mathbf{I}\mathbf{I}}]_{m \times n_2}$ is the dimensionless matrix of gains between \mathbf{I} and $\mathbf{I}_{\mathbf{NR}}$. Equation (9) can be used to model all the details of MCWPT systems. Hence, it is termed as the Detailed Model (DM). This matrix equation can be decoupled into two voltage path and current path sets of equations as in (10) and (11) respectively.

$$\begin{aligned} [\mathbf{E}] &= [\hat{\mathbf{G}}_{\mathbf{V}\mathbf{V}} \quad \hat{\mathbf{G}}_{\mathbf{I}\mathbf{V}}] \times \begin{bmatrix} \mathbf{V}_{\mathbf{TH}} \\ \mathbf{Z}_{\mathbf{NR}} \mathbf{I}_{\mathbf{NR}} \end{bmatrix} = \\ &[\hat{\mathbf{G}}_{\mathbf{V}\mathbf{V}} \quad \hat{\mathbf{G}}_{\mathbf{I}\mathbf{V}}] \times \begin{bmatrix} \mathbf{V}_{\mathbf{OC},\mathbf{VD}} \\ \mathbf{V}_{\mathbf{OC},\mathbf{CD}} \end{bmatrix} \end{aligned} \quad (10)$$

$$\begin{aligned} [\mathbf{I}] &= [\hat{\mathbf{G}}_{\mathbf{V}\mathbf{I}} \quad \hat{\mathbf{G}}_{\mathbf{I}\mathbf{I}}] \times \begin{bmatrix} \mathbf{Z}_{\mathbf{VD}}^{-1} \mathbf{V}_{\mathbf{TH}} \\ \mathbf{Z}_{\mathbf{CD}}^{-1} \mathbf{Z}_{\mathbf{NR}} \mathbf{I}_{\mathbf{NR}} \end{bmatrix} = \\ &[\hat{\mathbf{G}}_{\mathbf{V}\mathbf{I}} \quad \hat{\mathbf{G}}_{\mathbf{I}\mathbf{I}}] \times \begin{bmatrix} \mathbf{I}_{\mathbf{NC},\mathbf{VD}} \\ \mathbf{I}_{\mathbf{NC},\mathbf{CD}} \end{bmatrix} \end{aligned} \quad (11)$$

where $\mathbf{Z}_{\mathbf{CD}}$ is the diagonal matrix of overall impedances in CD coils, $\mathbf{Z}_{\mathbf{VD}}$ is the diagonal matrix of the VD coils overall impedances, $\mathbf{Z}_{\mathbf{NR}}$ is the diagonal matrix of the Norton impedances in CD coils, $\mathbf{V}_{\mathbf{OC},\mathbf{VD}} = \mathbf{V}_{\mathbf{TH}}$ and $\mathbf{V}_{\mathbf{OC},\mathbf{CD}} = \mathbf{Z}_{\mathbf{NR}} \mathbf{I}_{\mathbf{NR}}$ are the vectors of open circuit voltages in VD and CD coils respectively, and $\mathbf{I}_{\mathbf{NC},\mathbf{VD}} = \mathbf{Z}_{\mathbf{CD}}^{-1} \mathbf{V}_{\mathbf{TH}}$ and $\mathbf{I}_{\mathbf{NC},\mathbf{CD}} = \mathbf{Z}_{\mathbf{CD}}^{-1} \mathbf{Z}_{\mathbf{NR}} \mathbf{I}_{\mathbf{NR}}$ are the not-coupled currents of the VD and CD coils respectively. The obtained $\mathbf{G}_{\mathbf{V}\mathbf{V}}$, $\mathbf{G}_{\mathbf{I}\mathbf{I}}$, and $\mathbf{G}_{\mathbf{I}\mathbf{V}} = \mathbf{G}_{\mathbf{V}\mathbf{I}}$ form meaningful patterns between mutual inductances and overall impedances amongst the coils. To study these patterns, the three-coil MCWPT system, shown in Fig. 1 is analyzed in this subsection.

Therefore, by rearranging (6) to (8) according to (9), the following system of equations (which is sorted based on the independent (known) and dependent (unknown) electric variables) for the given three-coils system can be obtained.

$$\begin{aligned} \begin{bmatrix} E_1 \\ E_2 \\ E_3 \\ I_1 \\ I_2 \\ I_3 \end{bmatrix} &= \begin{bmatrix} -1 & 0 & 0 & 0 & L_{12}s & L_{13}s \\ 0 & -1 & 0 & L_{12}s & 0 & L_{23}s \\ 0 & 0 & -1 & L_{13}s & L_{23}s & 0 \\ -\frac{1}{Z_{11}} & 0 & 0 & -1 & 0 & 0 \\ 0 & -\frac{1}{Z_{22}} & 0 & 0 & -1 & 0 \\ 0 & 0 & 0 & -\frac{L_{13}s}{Z_3} & -\frac{L_{23}s}{Z_3} & -1 \end{bmatrix} \times \\ &\begin{bmatrix} 0 \\ 0 \\ 0 \\ -\frac{Z_{\mathbf{NR}1}}{Z_{11}} \\ 0 \\ 0 \end{bmatrix} \times \begin{bmatrix} I_{\mathbf{NR}1} \\ V_{\mathbf{TH}2} \end{bmatrix} \end{aligned} \quad (12)$$

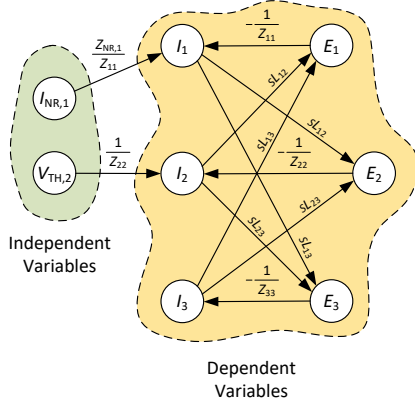


Fig. 7: Signal flow graph of the three-coil detailed model.

The signal flow graph representing (12) is shown in Fig. 7.

After solving (12), the induced voltages (E_i) and currents (I_i) for coils $i = 1, 2$ and 3 are to be found through (13) and (14) respectively.

$$\begin{bmatrix} E_1 \\ E_2 \\ E_3 \end{bmatrix} = \frac{1}{\Delta} \underbrace{\begin{bmatrix} \text{NVP}_{11} & \text{NVP}_{21} \\ \text{NVP}_{12} & \text{NVP}_{22} \\ \text{NVP}_{13} & \text{NVP}_{23} \end{bmatrix}}_{\text{Numerator of Voltage Path (NVP)}} \times \underbrace{\begin{bmatrix} V_{\text{TH}1}=V_{\text{OC},1} \\ Z_{\text{NR}1} I_{\text{NR}1} \\ V_{\text{TH}2} \\ V_{\text{OC},2} \end{bmatrix}}_{\text{Independent Variables}} \quad (13)$$

$$\begin{bmatrix} I_1 \\ I_2 \\ I_3 \end{bmatrix} = \frac{1}{\Delta} \underbrace{\begin{bmatrix} \text{NCP}_{11} & \text{NCP}_{21} \\ \text{NCP}_{12} & \text{NCP}_{22} \\ \text{NCP}_{13} & \text{NCP}_{23} \end{bmatrix}}_{\text{Numerator of Current Path (NCP)}} \times \underbrace{\begin{bmatrix} I_{\text{NC},1} \\ \left(\frac{Z_{\text{NR}1}}{Z_{11}} \right) I_{\text{NR}1} \\ \left(\frac{1}{Z_{22}} \right) V_{\text{TH}2} \\ I_{\text{NC},2} \end{bmatrix}}_{\text{Independent Variables}} \quad (14)$$

NVPs and NCPs in (13) and (14), are the numerator of voltage path and numerator of current path. Each of these numerators together with the characteristic function Δ form a graph set. Each graph set consists of a set of graphs which are represented by the sub-terms of NVPs, NCPs, and Δ . For the given three-coil system, the sub-terms of NVP, NCP, and Δ are given in Appendix A.

Moreover, $V_{\text{OC},i}$ is the voltage across the i^{th} coil source terminals, when it is open-circuited, and it is equal to $V_{\text{TH},i}$. Likewise, $I_{\text{NC},i}$ is the i^{th} coil current when there is no coupling in the system, and the induced voltage E_i is equal to zero.

The equations that link independent voltages and currents ($V_{\text{TH},i}$, $I_{\text{NR},i}$) to a dependent voltage (E_i) are called voltage path equations (13). Likewise, the equations that link independent voltages and currents ($V_{\text{TH},i}$, $I_{\text{NR},i}$) to a dependent current (I_i) are called current path equations (14). One can observe some meaningful patterns in the numerator of voltage path (NVP) equations, the numerator of current path (NCP) equations, and denominator of current path and voltage path equations. The denominator of all these transfer functions is identical, and it is called characteristic function (Δ). These

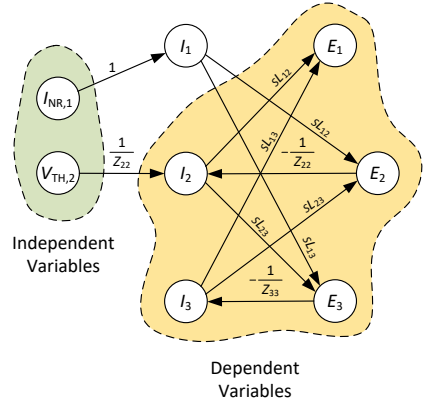


Fig. 8: Signal flow graph of the three-coil MCWPT system, in which CD coils are approximated (AP1).

NVP, NCP, and Δ terms are used as the basis of defining the GSM for MCWPT systems. $\text{NVP}_{ij}(k)$ refers to the numerator term corresponding to coils i and j for the k^{th} path in its graph set, $\text{NCP}_{ij}(k)$ represents the numerator term for the current path between coils i and j for the k^{th} path, and $\Delta(k)$ represents the denominator term for the k^{th} path. These terms, $\text{NVP}_{ij}(k)$, $\text{NCP}_{ij}(k)$, and $\Delta(k)$, will be used extensively to characterize the concept of GSM.

B. Approximation of CD Coils (AP1)

Using the similar approach as in DM and considering CD coils to be ideal ($Z_{\text{NR}} = Z_{11} \rightarrow \infty$), the first step of approximation is derived and called AP1. Therefore, the obtained governing matrix equation can be simplified into:

$$\begin{bmatrix} E_1 \\ E_2 \\ I_3 \end{bmatrix} = \begin{bmatrix} -1 & 0 & L_{12}s & L_{13}s \\ 0 & -1 & 0 & L_{23}s \\ 0 & -\frac{1}{Z_{22}} & -1 & 0 \\ 0 & 0 & -\frac{L_{23}s}{Z_{33}} & -1 \end{bmatrix}^{-1} \times \begin{bmatrix} 0 & 0 \\ -L_{12}s & 1 \\ 0 & -\frac{1}{Z_{22}} \\ \frac{L_{13}s}{Z_{33}} & 0 \end{bmatrix} \times \begin{bmatrix} I_{\text{NR}1} \\ V_{\text{TH}2} \end{bmatrix} \quad (15)$$

For clarity, E_3 in (12) is removed in the process of simplification of (15) as it can be easily obtained by $E_3 = -Z_{33}I_3$.

This system yields the signal flow graph shown in Fig. 8. As long as the system behaves as a CD coil in steady state mode at its tuned frequency ω_0 ($s = j\omega_0$), (15) can be used to represent all types of coils. For example, a system equipped with an LCC compensator can only show the current source features at its tuning frequency, whereas at other frequencies, this behavior is not achievable.

C. Approximation of CD and VD Coils (AP2)

The next step of simplification belongs to both CD and VD coils, and it is termed as AP2. In this stage, it is assumed that both CD and VD coils are ideal, where $Z_{\text{NR},i} \rightarrow \infty$. $Z_{ii} = Z_{\text{TH},i} + Z_i = 0$. Therefore, DM will be simplified to (16), which is obtained from the three main equations of (17) to (19).

For constant driving frequency of ω_0 , (16) can be used to simplify all types of VD and CD coils as long as the assumption of their ideal behavior is valid at ω_0 .

$$\begin{bmatrix} E_1 \\ I_2 \\ I_3 \end{bmatrix} = \begin{bmatrix} -1 & L_{12}s & L_{13}s \\ 0 & 0 & L_{23}s \\ 0 & -\frac{L_{23}s}{Z_{33}} & -1 \end{bmatrix}^{-1} \times \begin{bmatrix} 0 & 0 \\ -L_{12}s & 1 \\ \frac{L_{13}s}{Z_{33}} & 0 \end{bmatrix} \times \begin{bmatrix} I_{NR1} \\ V_{TH2} \end{bmatrix} \quad (16)$$

$$E_1 = L_{12}sI_2 + L_{13}sI_3 \quad (17)$$

$$V_{TH2} = L_{12}sI_{NR1} + L_{23}sI_3 \quad (18)$$

$$E_3 = -Z_{33}I_3 = L_{13}sI_{NR1} + L_{23}sI_2 \quad (19)$$

D. Approximation with the Omission of Negligible Couplings (AP3)

The purpose of this approximation is to reduce the number of graphs in each graph set and simplify the GSM analysis. This stage of approximation is carried out with the omission of negligible coupling terms for a given system. Therefore, the MCWPT system will be modelled with the use of dominant couplings in the graph sets. As an example, in the given system shown in Fig. 1, the coupling term L_{13} is much weaker than other couplings. Therefore, it can be neglected in AP3.

E. Categorization of Graph Sets

As it is shown in Figs. 7 and 8, the complexity of the obtained signal flow graphs can be exponentially increased by the increase in the number of coils. This is due to having both current and voltage dependent variables in the same graphical representation. Therefore, aiming for reduction of this complexity, the graph sets are separately obtained for each coil, and as a result, the graph sets are formed based on only overall impedances and mutual inductances, which helps finding the effective patterns amongst the coils to transfer the power. These graph sets can be categorized into three basic sets, namely loops, transferred graph sets, and reflected graph sets. Loops (LPs) do not have sourcing and sinking coils and they can be enclosed between different number of coils. Transferred graph sets consist of a path starting from a sourcing coil i and ending up at a sinking coil j .

Reflected graph sets have paths sourcing and sinking the same coil. For reflected graph sets, there are two sub-categories of attached and isolated sets. If the sourcing (and sinking) coil contri

reflected graph set (P_{ii}), and if sourcing (and sinking coil) does not form any path amongst the rest of the coils, it is called isolated reflected graph set (\bar{P}_{ii}). For both P_{ii} and \bar{P}_{ii} , the coils that do not contribute to the paths can form different possible arrangements of loops. Using these graph sets and the symbols shown in Fig. 6, this section shows how graph sets can be derived from DM, AP1, AP2, and AP3 of an MCWPT system. In the subsequent section, each of these graph sets are elaborated.

Interestingly, all the possible graph sets can be found from DM, which can be used to fully characterize the MCWPT. In the process of approximating DM, the methods AP1, AP2, and AP3 are used and some graphs are removed in each approximation step. Δ , NCPs, and NVPs are shown in Tables I to VIII. The first row of these Tables represents the graph set index (k). (e.g. LP(k) is the loop graph of (k) for the k^{th} term in the denominators of (13) and (14), and P(k) stands for the graphs of NCP(k) or NVP(k) for its respective k^{th} term in the numerator). In the second row, the graphical representation of all graph sets obtained from (13) and (14) is shown. The third, fourth, fifth, and sixth rows show the graph sets for the DM, AP1, AP2, and AP3 respectively. These rows show different simplifications of the system in each scenario. The simplification steps are detailed in the foot notes (\dagger , \ddagger , $*$, $**$, and $\#$).

IV. GENERAL RULES FOR REALISTIC GRAPH SETS

Based on the simplifications and the discussions in the previous section, several rules for the graph sets are formulated. The rules of an MCWPT system, consisting of multiple active and passive coils can be summarized as in the following subsections.

A. Characteristic Function of a MCWPT System Δ

According to what has been obtained from (13) and (14), denominator of the graph set terms can be written as in (20).

$$\Delta = \sum_{k=1}^n \Delta(k) \quad (20)$$

where k is the index of the graph set loops, and n is the maximum number of possible loops in the graph sets of the , there are

	LP(1) for $\Delta(1)$	LP(2) for $\Delta(2)$	LP(3) for $\Delta(3)$	LP(4) for $\Delta(4)$	LP(5) for $\Delta(5)$
GS					
DM	1	$-\frac{L_{13}^2 s^2}{ Z_{11} Z_{33}}$	$-\frac{L_{23}^2 s^2}{Z_{22}Z_{33}}$	$-\frac{L_{12}^2 s^2}{ Z_{11} Z_{22}}$	$\frac{2L_{12}L_{13}L_{23}s^3}{ Z_{11} Z_{22}Z_{33}}$
AP1	1	0 ^(†)	$-\frac{L_{23}^2 s^2}{Z_{22}Z_{33}}$	0 ^(†)	0 ^(†)
AP2	0 ^(*)	0 ^(*)	$-\frac{L_{23}^2 s^2}{ Z_{22} Z_{33}}$	0 ^(*)	0 ^(*)
AP3	1	0 ^(**)	$-\frac{L_{23}^2 s^2}{Z_{22}Z_{33}}$	$-\frac{L_{12}^2 s^2}{Z_{11}Z_{22}}$	0 ^(**)

	$P_{11}(1)$ for $NVP_{11}(1)$	$P_{11}(2)$ for $NVP_{11}(2)$	$P_{11}(3)$ for $NVP_{11}(3)$	$P_{21}(1)$ for $NVP_{21}(1)$	$P_{21}(2)$ for $NVP_{21}(2)$
GS					
DM	$-\frac{L_{12}^2 s^2}{[Z_{11}]Z_{22}} [Z_{NR1}] I_{NR1}$	$-\frac{L_{13}^2 s^2}{[Z_{11}]Z_{33}} [Z_{NR1}] I_{NR1}$	$\frac{2L_{12}L_{23}L_{13} s^3}{[Z_{11}]Z_{22}Z_{33}} [Z_{NR1}] I_{NR1}$	$\frac{L_{12} s}{Z_{22}} V_{TH2}$	$-\frac{L_{13}L_{23} s^2}{Z_{22}Z_{33}} V_{TH2}$
AP1	$-\frac{L_{12}^2 s^2}{Z_{22}} I_{NR1}^{(*)}$	$-\frac{L_{13}^2 s^2}{Z_{33}} I_{NR1}^{(*)}$	$\frac{2L_{12}L_{23}L_{13} s^3}{Z_{22}Z_{33}} I_{NR1}^{(*)}$	$\frac{L_{12} s}{Z_{22}} V_{TH2}$	$-\frac{L_{13}L_{23} s^2}{Z_{22}Z_{33}} V_{TH2}$
AP2	$-\frac{L_{12}^2 s^2}{Z_{22}} I_{NR1}^{(*)}$	$0^{(*)}$	$\frac{2L_{12}L_{23}L_{13} s^3}{Z_{22}Z_{33}} I_{NR1}^{(*)}$	$\frac{L_{12} s}{Z_{22}} V_{TH2}$	$-\frac{L_{13}L_{23} s^2}{Z_{22}Z_{33}} V_{TH2}$

	$\bar{P}_{11}(1)$ for $NCP_{11}(1)$	$\bar{P}_{11}(2)$ for $NCP_{11}(2)$	$P_{21}(1)$ for $NCP_{21}(1)$	$P_{21}(2)$ for $NCP_{21}(2)$
GS				
DM	$\frac{[Z_{NR1}]}{[Z_{11}]} I_{NR1}$	$-\frac{L_{23}^2 s^2}{Z_{22}Z_{33}} \frac{[Z_{NR1}]}{[Z_{11}]} I_{NR1}$	$-\frac{L_{12} s}{[Z_{11}]} V_{TH2}$	$\frac{L_{13}L_{23} s^2}{[Z_{11}]Z_{33}} \frac{V_{TH2}}{Z_{22}}$
AP1	$\frac{[Z_{NR1}]}{[Z_{11}]} I_{NR1}^{(*)}$	$-\frac{L_{23}^2 s^2}{Z_{22}Z_{33}} I_{NR1}^{(*)}$	$0^{(*)}$	$0^{(*)}$
AP2	$0^{(*)}$	$-\frac{L_{23}^2 s^2}{Z_{22}Z_{33}} I_{NR1}^{(*)}$	$0^{(*)}$	$0^{(*)}$

	$P_{22}(1)$ for $NVP_{22}(1)$	$P_{22}(2)$ for $NVP_{22}(2)$	$P_{22}(3)$ for $NVP_{22}(3)$	$P_{12}(1)$ for $NVP_{12}(1)$	$P_{12}(2)$ for $NVP_{12}(2)$
GS					
DM	$-\frac{L_{12}^2 s^2}{[Z_{11}]Z_{22}} V_{TH2}$	$-\frac{L_{23}^2 s^2}{Z_{22}Z_{33}} V_{TH2}$	$\frac{2L_{12}L_{23}L_{13} s^3}{[Z_{11}]Z_{22}Z_{33}} V_{TH2}$	$\frac{L_{12} s}{[Z_{11}]} [Z_{NR1}] I_{NR1}$	$-\frac{L_{13}L_{23} s^2}{[Z_{11}]Z_{33}} [Z_{NR1}] I_{NR1}$
AP1	$0^{(*)}$	$-\frac{L_{23}^2 s^2}{Z_{22}Z_{33}} V_{TH2}^{(*)}$	$0^{(*)}$	$\frac{L_{12} s}{[Z_{11}]} I_{NR1}^{(*)}$	$-\frac{L_{13}L_{23} s^2}{Z_{33}} I_{NR1}^{(*)}$
AP2	$0^{(*)}$	$-\frac{L_{23}^2 s^2}{Z_{22}Z_{33}} V_{TH2}^{(*)}$	$0^{(*)}$	$0^{(*)}$	$0^{(*)}$

	$\bar{P}_{22}(1)$ for $NCP_{22}(1)$	$\bar{P}_{22}(2)$ for $NCP_{22}(2)$	$P_{12}(1)$ for $NCP_{12}(1)$	$P_{12}(2)$ for $NCP_{12}(2)$
GS				
DM	$\frac{V_{TH2}}{Z_{22}}$	$-\frac{L_{13}^2 s^2}{[Z_{11}]Z_{33}} \frac{V_{TH2}}{Z_{22}}$	$-\frac{L_{12} s}{Z_{22}} \frac{[Z_{NR1}]}{[Z_{11}]} I_{NR1}$	$\frac{L_{13}L_{23} s^2}{Z_{22}Z_{33}} \frac{[Z_{NR1}]}{[Z_{11}]} I_{NR1}$
AP1	$\frac{V_{TH2}}{Z_{22}}$	$0^{(*)}$	$-\frac{L_{12} s}{Z_{22}} I_{NR1}^{(*)}$	$\frac{L_{13}L_{23} s^2}{Z_{22}Z_{33}} I_{NR1}^{(*)}$
AP2	$\frac{V_{TH2}}{[Z_{22}]}$	$0^{(*)}$	$-\frac{L_{12} s}{[Z_{22}]} I_{NR1}^{(*)}$	$\frac{L_{13}L_{23} s^2}{[Z_{22}]Z_{33}} I_{NR1}^{(*)}$
AP3	$\frac{V_{TH2}}{Z_{22}}$	$0^{(**)}$	$-\frac{L_{12} s}{Z_{22}} \frac{[Z_{NR1}]}{Z_{11}} I_{NR1}$	$0^{(**)}$

	$P_{13}(1)$ for $NVP_{13}(1)$	$P_{13}(2)$ for $NVP_{13}(2)$	$P_{23}(1)$ for $NVP_{23}(1)$	$P_{23}(2)$ for $NVP_{23}(2)$
GS				
DM	$\frac{L_{13}s}{ Z_{11} } [Z_{NR1}] I_{NR1}$	$-\frac{L_{12}L_{23}s^2}{ Z_{11} Z_{22}} [Z_{NR1}] I_{NR1}$	$\frac{L_{23}s}{Z_{22}} V_{TH2}$	$-\frac{L_{12}L_{13}s^2}{ Z_{11} Z_{22}} V_{TH2}$
AP1	$L_{13}s I_{NR1}$	$-\frac{L_{12}L_{23}s^2}{Z_{22}} I_{NR1} (\ddagger)$	$\frac{L_{23}s}{Z_{22}} V_{TH2}$	$0^{(\ddagger)}$
AP2	$0^{(*)}$	$-\frac{L_{12}L_{23}s^2}{ Z_{22} } I_{NR1} (\ddagger)$	$\frac{L_{23}s}{ Z_{22} } V_{TH2}$	$0^{(*)}$

	$P_{13}(1)$ for $NCP_{13}(1)$	$P_{13}(2)$ for $NCP_{13}(2)$	$P_{23}(1)$ for $NCP_{23}(1)$	$P_{23}(2)$ for $NCP_{23}(2)$
GS				
DM	$-\frac{L_{13}s}{Z_{33}} \frac{ Z_{NR1} }{ Z_{11} } I_{NR1}$	$\frac{L_{12}L_{23}s^2}{Z_{22}Z_{33}} \frac{ Z_{NR1} }{ Z_{11} } I_{NR1}$	$-\frac{L_{23}s}{Z_{33}} \frac{1}{Z_{22}} V_{TH2}$	$\frac{L_{12}L_{13}s^2}{ Z_{11} Z_{33}} \frac{1}{Z_{22}} V_{TH2}$
AP1	$-\frac{L_{13}s}{Z_{33}} I_{NR1} (\ddagger)$	$\frac{L_{12}L_{23}s^2}{Z_{22}Z_{33}} I_{NR1} (\ddagger)$	$-\frac{L_{23}s}{Z_{33}} \frac{1}{Z_{22}} V_{TH2}$	$0^{(\ddagger)}$
AP2	$0^{(*)}$	$\frac{L_{12}L_{23}s^2}{ Z_{22} Z_{33}} I_{NR1} (\ddagger)$	$-\frac{L_{23}s}{Z_{33}} \frac{1}{ Z_{22} } V_{TH2}$	$0^{(*)}$

	$P_{33}(1)$ for $NVP_{33}(1)$	$P_{33}(2)$ for $NVP_{33}(2)$	$P_{33}(3)$ for $NVP_{33}(3)$	$\bar{P}_{33}(1)$ for $NCP_{33}(1)$	$\bar{P}_{33}(2)$ for $NCP_{33}(2)$
GS					
DM	$-\frac{L_{13}^2s^2}{ Z_{11} Z_{13}} V_{TH3}^*$	$-\frac{L_{23}^2s^2}{Z_{22}Z_{33}} V_{TH3}^*$	$\frac{2L_{12}L_{23}L_{13}s^3}{ Z_{11} Z_{22}Z_{33}} V_{TH3}^*$	$\frac{1}{Z_{33}} V_{TH3}^*$	$-\frac{L_{13}^2s^2}{ Z_{11} Z_{22}} \frac{1}{Z_{33}} V_{TH3}^*$
AP1	$0^{(\ddagger)}$	$-\frac{L_{23}^2s^2}{Z_{22}Z_{33}} V_{TH3}^*$	$0^{(\ddagger)}$	$\frac{1}{Z_{33}} V_{TH3}^*$	$0^{(\ddagger)}$
AP2	$0^{(*)}$	$-\frac{L_{23}^2s^2}{ Z_{22} Z_{33}} V_{TH3}^*$	$0^{(*)}$	$\frac{1}{Z_{33}} V_{TH3}^*$	$0^{(*)}$
AP3	$0^{(**)}$	$-\frac{L_{23}^2s^2}{Z_{22}Z_{33}} V_{TH3}^*$	$0^{(**)}$	$\frac{1}{Z_{33}} V_{TH3}^*$	$0^{(**)}$

† In AP1, for the i^{th} ideal CD coil, $Z_{NR,i} \rightarrow \infty$ and $Z_{ii} = Z_{NR,i} + Z_i \rightarrow \infty$. Therefore, the presence of Z_{ii} in the denominator of NVP, NCP, and Δ terms will make the respective terms approach zero and to be unimportant in the graph sets. Consequently, the graphs associated with the highlighted cells marked by (†) are canceled out for AP1.

‡ Referring to the same reason explained in (†) for AP1, when $Z_{NR,i} \rightarrow \infty$, $\frac{Z_{NR,i}}{Z_{ii}} \rightarrow 1$. Therefore, for the graphs that are marked by (‡), $Z_{NR,i}$ in the numerator cancels out Z_{ii} in the denominator.

* In the second step of approximation AP2 for the i^{th} ideal VD coil, $Z_{ii} = Z_{TH,i} + Z_i \rightarrow 0$. Therefore, the terms containing Z_{ii} in their denominator become significantly larger than the other terms and make the effect of other terms to be negligible. Worthy to mention that, as this term is present in NVP, NCP, and Δ , they will be cancelled out in the numerator and denominator of both voltage path equations and current path equations and can be removed from the AP3 of the NVP, NCP, and Δ graph sets. The terms that are overwhelmed by Z_{ii} -possessed terms are removed from the graph sets, and they are highlighted and marked by (*).

** In the third step of approximation AP3, graphs contributing to the negligible mutual inductances are removed. These graphs are highlighted and shown by (**). Worthy to mention that, AP3 is directly obtained from DM.

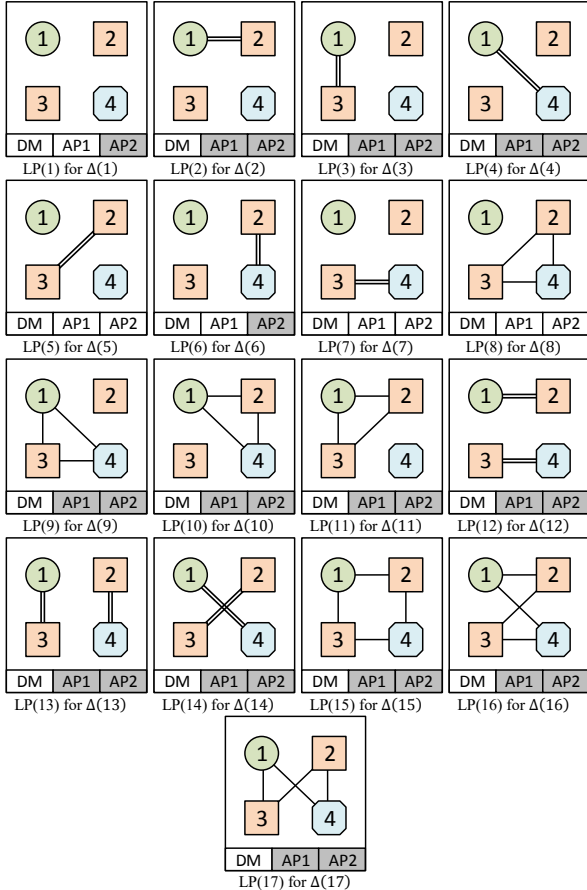
V_{TH3}^* is the virtual source voltage, which drives the passive coil 3. This voltage source is used to investigate how the reflected impedance seen from passive coil is derived.

four possible loops in its graph sets. obtained from (21).

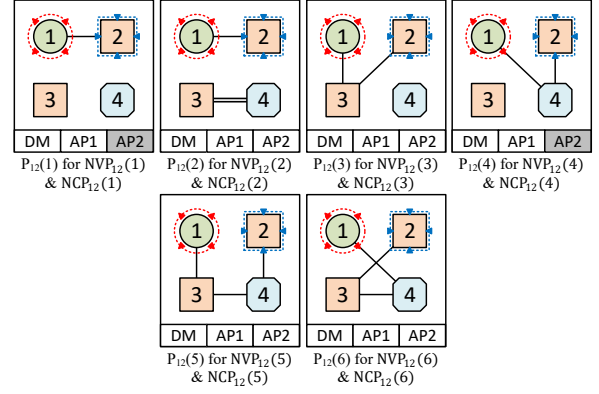
$$\Delta(k) = \begin{cases} 1; \\ 2^a \times (-1)^\alpha \times (j\omega)^\rho \times g_\delta(\text{LP}(k)) \end{cases}$$

where a is the number of loops enclosed, α is the number of lines in the of loops, and ρ is the number of li represents the graph of the k^{th} loop g_δ is the graph set equation of the $g_\delta(\text{LP}(k)) = \prod L_{ij} / \prod Z_{mm}$, where \prod mutual inductances forming $\text{LP}(k)$, ε overall impedance that is contributed (coil) is touched for many times by di its overall impedance must be writte denominator). The resultant $\Delta(k)$ for three-coil system is shown in Table I. example of LP sets for a four-coil MC of one CD coil (coil 1), two VD coils (coils 2 and 3) and one PS coil (coil 4), and the removed graph sets for each step of approximation is shaded in gray. Δ terms of this system is given in Appendix B.

TABLE IX: An example of $\text{LP}(k)$ graph sets for Δ in a four-coil MCWPT system.



As mentioned in the footnotes of the tables, ((†), (‡), and (*)), ideal CD coils do not involve in any loop, and on the contrary ideal VD coil must be included in all loops. Therefore, the number of graphs for characteristic function



loops can be significantly decreased during the different stages of approximation. This can be seen in Tables I and IX.

B. Transferred Voltage

Voltage across a particular coil consists of two different components, which are termed as transferred voltage ($(\text{NVP}_{ij}/\Delta) V_{\text{OC},i}$) and reflected voltage ($(\text{NVP}_{ii}/\Delta) V_{\text{OC},i}$). Transferred voltage appears across the concerned coil i due to the induced voltage as a result of other neighboring source excitations ($I_{\text{NR},j}$ or $V_{\text{TH},j}$). This can occur directly or indirectly through the other coils. NVP_{ij} for the transferred voltage from active coil i and received by coil j can be written as follows:

$$\text{NVP}_{ij} = \sum_{k=1}^n \text{NVP}_{ij}(k) \quad (22)$$

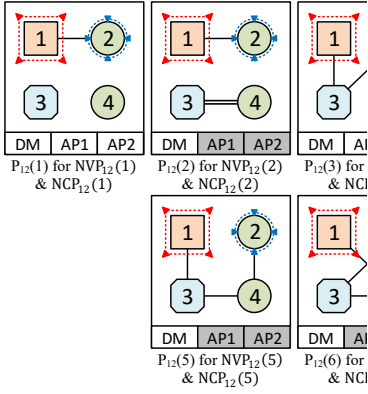
where n is the maximum possible number of NVP_{ij} graphs, and k is the graph set index. $\text{NVP}_{ij}(k)$ is

$$\text{NVP}_{ij}(k) = 2^a \times (-1)^{\alpha+1} \times (j\omega)^\rho \times g_v(\text{P}_{ij}(k)) \quad (23)$$

where a , α , ρ , and g_v are identical to what has been explained in (21). $\text{P}_{ij}(k)$ is the k^{th} graph which forms a path linking coil i to the coil j . Other coils that are not included in the path between coils i and j can form different arrangements of loops for each k index. **Furthermore, for g_v of $\text{NVP}_{ij}(k)$, the overall impedance of the sinking coil j (Z_{jj}) is not included in the denominator.** Tables II, IV, and VI show different graph sets for NVP between two different coils.

For better understanding how graph sets are formed for a transferred voltage between two coils, two different four-coil MCWPT systems are provided as extra examples in Tables X and XI. Table X shows $\text{P}_{12}(k)$ for the k^{th} graph set between coils 1 and 2 in an MCWPT system consisting of one CD coil (coil 1), two VD coils (coils 2 and 3) and one PS coil (coil 4). Similarly, different graphs of P_{12} graph set are shown in Tables XI for a four-coil WPT system, which comprises of two CD coils (coils 2 and 4), one VD coil (coil 1), and one PS coil (coil 3). NVP_{12} terms of these systems are identical, and they are given in Appendix C.

According to (†) and (‡), for the i^{th} ideal CD coil, Z_{ii} tends to infinity, and therefore NVP_{ij} terms having Z_{ii} in their



denominator will approach zero and graph sets for AP1, as shown for sl and XI. Referring to (*) for the i approaches zero, and it makes the N their denominator to be dominant. The other terms can be neglected as shaded AP2 shows in Tables II and XI. Along with the use of similar indicators to distinguish different steps of approximation for AP1 and AP2, another indicator is assigned to AP3 to show the removed graphs as a result of negligible couplings.

C. Reflected Voltage

The other component in voltage of a particular coil is the reflected voltage $(NVP_{ii}/\Delta)V_{OC,i}$. Reflected voltage is generated due to the voltage induced in the neighboring coils as a result of excitation in the concerned coil ($I_{NR,i}$ or $V_{TH,i}$). This induced voltage in the neighboring coils creates a current, and it will in turn induce a voltage in the coil under study, which is termed as the reflected voltage.

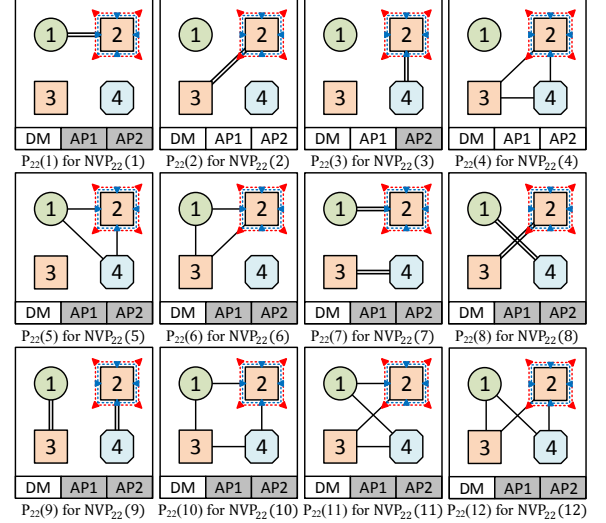
For the sourcing coil and receiving coil i , NVP_{ii} can be written as follows:

$$NVP_{ii} = \sum_{k=1}^n NVP_{ii}(k) \quad (24)$$

where n is the maximum possible NVP_{ii} graphs when the i^{th} coil is sourcing and sinking at the same time, and k is the graph set index. $NVP_{ii}(k)$ is

$$NVP_{ii}(k) = 2^a \times (-1)^\alpha \times (j\omega)^\rho \times g_\delta(P_{ii}(k)) \quad (25)$$

where a , α , ρ , and g_δ are identical to what has been explained in (21), except that the attached reflected path $P_{ii}(k)$ is treated as a loop. $P_{ii}(k)$ is the graph of the k^{th} attached reflected path. When the i^{th} coil forms its P_{ii} graph set, other coils that are not involved in its loop can take different loops in the graph sets. The graph set of P_{ii} for the given three-coil system is shown in Tables II, IV, and VIII. For better understanding how the NVP_{ii} graph set is formed, another example for a four-coil system comprising of one CD coil (coil 1), two VD coils (coils 2 and 3), and one passive coil (coil 4) is



given in Table XII. NVP_{22} terms of this system are given in Appendix D. As it can be seen in Table XII, the second coil enclosing its path amongst different coils, and the other uninvolved coils can form different loop arrangements. Based on (\dagger) and (\ddagger), considering CD coil as an ideal coil in AP1, the shaded AP1 graphs in Tables II, IV, VIII, and XII can be removed. According to (*), having the assumption of ideal CD and VD coils in AP2, the effect of shaded AP2 graphs in these tables can be removed.

D. Transferred Current

Current in a particular coil consists of two different components, which are termed as transferred current $(NCP_{ij}/\Delta)I_{NC,i}$ and reflected current $(NCP_{ii}/\Delta)I_{NC,i}$. Transferred current is flown in the concerned coil j due to the induced voltage as a result of other neighboring source excitations ($I_{NR,j}$ or $V_{TH,j}$). This can occur directly or indirectly through the other coils. NCP_{ij} for the transferred current from active coil i and received by coil j can be written as follows:

$$NCP_{ij} = \sum_{k=1}^n NCP_{ij}(k) \quad (26)$$

where n is the all possible NCP_{ij} graphs, and k is the graph set index. $NCP_{ij}(k)$ is

$$NCP_{ij}(k) = 2^a \times (-1)^\alpha \times (j\omega)^\rho \times g_i(P_{ij}(k)) \quad (27)$$

where a , α , and ρ , are similar to what has been explained in (21). $P_{ij}(k)$ for the k^{th} graph of NCP_{ij} is identical to NVP_{ij} , and it includes a path linking coils i to j , and all possible loops between the coils that are not included in the path. Unlike transferred voltage, in g_i of NCP_{ij} , the overall impedance of the sourcing coil i is not included in the denominator of the GSM equation g_i . NCP_{ij} between different coils of the three-coil MCWPT system is shown in Tables III, V, VII, X, and XI. The NCP_{12} terms associated with the MCWPT

systems shown in Tables X and XI a given in Appendix E.

E. Reflected Current in Active Coils

The other current component of reflected current (NCP_{ii}/Δ) $I_{\text{NC},i}$. Related due to the voltage induced in a result of excitation in the concern. This induced voltage in the neighbor current in those coils, and it will in the coil i . The induced voltage in the produce a current in the same coil, reflected current. Therefore, the presence of coils influences the excited coil current for NCP_{ii} is similar to what has characteristic function Δ . NCP_{ii} can be

$$\text{NCP}_{ii} = \sum_{k=1}^n \text{NCP}_{ii}(k)$$

where n is the maximum possible NC graph set index. $\text{NCP}_{ij}(k)$ is

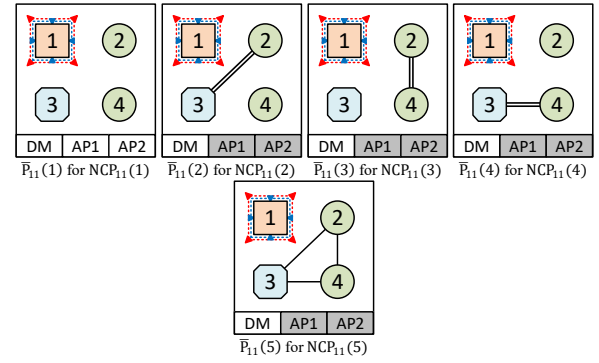
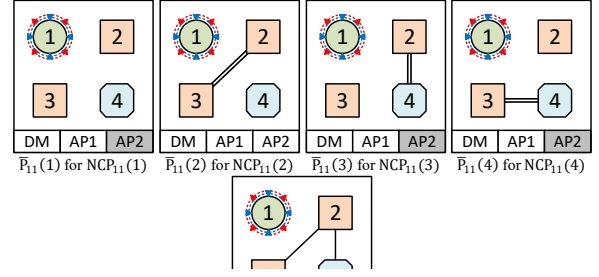
$$\text{NCP}_{ii}(k) = \begin{cases} 1; \\ 2^a \times (-1)^\alpha \times (j\omega)^\rho \times g_\delta \end{cases}$$

where a , α , ρ , and g_δ are identical to in (21), except that all isolated reflectors as loops. $\bar{P}_{ii}(k)$ is the k^{th} isolated when coil i overall impedance (Z_{ii}) is $\text{NCP}_{ii}(k)$ for different loops of the three-coil system is shown in the third row of Tables III, V, and VIII.

As for further examples, Tables XIII and XIV, show $\bar{P}_{ii}(k)$ graph sets for NCP of reflected current graph sets in coil 1 (NCP_{11}) in the four-coil MCWPT systems proposed in Tables XI and XII respectively. As previously mentioned, in these graph sets, the sourcing coil does not participate in the loops. Therefore, in a specific MCWPT system, the number of loops for the reflected current graph sets is lower than its characteristic function loops. Furthermore, similar to what has been explained for the loops of Δ in (\dagger) and (\ddagger), in the reflected current loops, ideal CD coils are not included in the loops, and according to ($*$) for ideal VD coils, they must contribute to the loops. As a result, the removed graph sets for AP1 and AP2 are shaded in Tables III, V, VIII, XIII, and XIV. NCP_{11} terms of the MCWPT systems shown in Tables XIII and XIV are identical, and they are given in Appendix F.

V. GAIN PARAMETERS OF THE MCWPT SYSTEM

Once all the graph sets are formed, an MCWPT system can be characterized by three different types of gains, namely gain of voltage path between coils i and j (GVP_{ij}), gain of current path between coils i and j (GCP_{ij}), and reflected impedance ($Z_{rfl,ii}$). As explained in (9) and (11), these gains can be obtained as follows:



$$\text{GVP}_{ij} = \begin{cases} \hat{g}_{vv,ij} = \frac{\text{NVP}_{ij}}{\Delta}; & j \text{ is VD} \\ \hat{g}_{vi,ij} = Z_{\text{NR},j} \hat{g}_{vi,ij} = Z_{\text{NR},j} \frac{\text{NVP}_{ij}}{\Delta}; & j \text{ is CD} \end{cases} \quad (30)$$

$$\text{GCP}_{ij} = \begin{cases} g_{iv,ij} = Z_{jj}^{-1} \hat{g}_{iv,ij} = Z_{jj}^{-1} \frac{\text{NCP}_{ij}}{\Delta}; & j \text{ is VD} \\ \frac{Z_{\text{NR},i}}{Z_{jj}} g_{ii,ij} = \frac{Z_{\text{NR},i}}{Z_{jj}} \frac{\text{NCP}_{ij}}{\Delta}; & j \text{ is CD} \end{cases} \quad (31)$$

where $\hat{g}_{iv,ij}$ and $\hat{g}_{ii,ij}$, and $\hat{g}_{vv,ij}$ are the dimensionless elements of $\hat{\mathbf{G}}_{IV}$, $\hat{\mathbf{G}}_{VV}$, and $\hat{\mathbf{G}}_{VV}$ matrices explained in (10) and (11) respectively, and while sourcing coil j supplies sinking coil i . Similarly, $g_{iv,ij}$ and $g_{vi,ij}$ are the components of G_{IV} and G_{VI} matrices.

Reflected impedance is the impedance of other surrounding coils seen from the i^{th} coil terminals. This impedance can be obtained by dividing the gain of voltage path of the reflected voltage, GVP_{ii} , by the gain of current path of the reflected current, GCP_{ii} as follows:

$$Z_{rfl,ii} = \frac{\text{GVP}_{ii}}{\text{GCP}_{ii}} = Z_{ii} \frac{\text{NVP}_{ii}}{\text{NCP}_{ii}} \quad (32)$$

In this way, reflected impedance for the active coils can be found as in (32). However, as there is no source in PS coils, the reflected impedance from the active coils to a passive coil i , can be obtained by replacing its load (R_L) by a virtual voltage or current source (Fig. 2(c)). For the given three-coil WPT system, V_{TH3}^* functions as a virtual voltage source, and its resultant graph sets are shown in Table VIII. The reflected impedances for coils 1, 2 and 3, and for DM, AP1, AP2, and AP3 are given in Appendix G.

VI. SUMMARY OF THE PROPOSED GRAPH SETS METHOD

So far it has been seen that graph sets are obtained from the Kirchhoff's principles, and similar to Mason's laws, GSM can graphically represent the interaction between coil couplings and overall impedances in an MCWPT system. Although the standard model can yield some valuable information, such as eigenvalues, eigenvectors, sensitivity, stability, controllability, and observability, the exact patterns of couplings and overall impedances responsible for dominant behavior of the system are not directly achievable. This can only be done by parametrically solving the whole system and finding out how the building blocks of the system (couplings and overall impedances) interact with each other. For instance, which combination of mutual inductances and overall impedances in an MCWPT system are responsible for change of phase angle between voltage and current in a sourcing coil i cannot be easily answered without a parametric equation between coil i voltage and current. Similarly, the advantageous and disadvantageous combinations of couplings and overall impedances in a repeater MCWPT system can be identified and the WPT process can be refined more effectively. The number of graphs in an MCWPT system, however, can exponentially increase with the increase in the number of coils, and as a result, in case of manually deriving the graph sets, some patterns may be overlooked. Hence, the approximation steps are proposed to simplify the system and to scale it down to its dominant patterns.

Therefore, similar to Mason's theory, this method can directly result in the dependent variables (outputs) to independent variable (inputs) gains, and one does not need to do the complex calculations to achieve the gains by parametrically solving the whole standard model equations (similar to (1) to (5)). Besides, establishing the GSM laws to form the graph sets, the system gains can be obtained through a set of laws which decreases the chance of missing some patterns.

The flowchart in Fig. 9 summarises the steps and the design procedure of the proposed GSM. In order to analyze an MCWPT system based on the proposed GSM, there are four main steps of (a) identifying the system, (b) categorizing the coils, (c) forming graph sets, and (d) analyzing and simplifying. Therefore, the main goal of GSM is to characterize, simplify, and analyze MCWPT systems to study their behavior. In addition to its computational advantages, GSM can be used to investigate the effect of couplings and impedances on the flow of power and reflected impedances.

Here, the following steps are used to briefly explain the GSM. In step (a), the system parameters, such as mutual inductance profiles, compensating capacitors and inductors, load, and ESRs need to be evaluated. In step (b), the coils are categorized into three different types of VD, CD, and PS coils based on their behavior. The compensator and its source define the type of active coils. Based on the type of a coil, its $Z_{NR,i}$, $Z_{TH,i}$, and Z_{ii} can be calculated in this step. According to the general rules for GSM, step (c) forms graph sets for Δ , NVPs, and NCPs. The expressions for their GVPs and GCPs can be obtained in the next step. In the final step of (d), GVPs, GCPs, and Δ can be simplified by either finding out

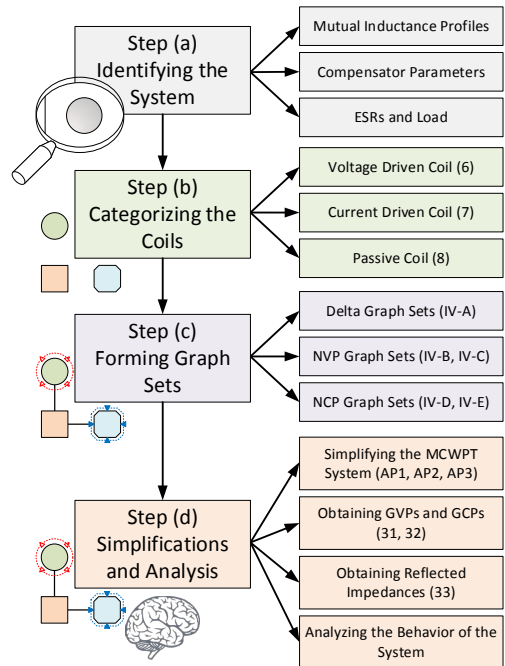


Fig. 9: GSM flowchart to analyze an MCWPT system.

the dominant sub-terms in NVPs, NCPs, and Δ or CD and VD approximations (or both) explained in Section III. Using these simplifications, the behavior of the system, in terms of flow of power, reflection of impedances, and its dynamic behavior can be analyzed, which is detailed in Part II of this paper.

VII. CONCLUSION

A new approach, *Graph Sets Method* (GSM), for modeling and analyzing MCWPT system is proposed in this article. The method is inspired by Mason's rule used in linear control systems, and it can be used to formulate MCWPT systems in a more knowledgeable way. For this purpose, WPT coils and their driving systems are classified into three different types of current driven, voltage driven, and passive coils. Then, with the use of Norton and Thevenin equivalents, the detailed models of the coils are formulated and used to reach the parametric solution of the system. *Graph sets* can be formed by the obtained solution, and some general rules can be obtained to form the current and voltage transfer functions between different coils. The proposed GSM can form the characteristic function and the gains between electric variables of the system. Moreover, the graph sets can be further simplified with the assumption of ideal current driven and voltage driven coils and removing the effect of negligible couplings. This approach can also formulate the reflected impedances seen from different coils. Therefore, in this paper, the principles of the graph sets method to model, analyze, and simplify MCWPT system are established. In the next part of this paper, to prove the validity and capabilities of this approach, a three-coil system, consisting of all three different type of CD, VD, and PS coils, is numerically analyzed using the GSM approach, and the obtained results are compared with the experimental results. It will be shown that the obtained results are consistent with the experimental results, and GSM can be used as an effective approach to analyze WPT systems.

APPENDIX A

$$\begin{aligned}
\text{NVP}_{11} &= -\underbrace{\frac{L_{12}^2 s^2}{Z_{11} Z_{22}}}_{\text{NVP}_{11}(1)} + \underbrace{\frac{L_{13}^2 s^2}{Z_{11} Z_{33}}}_{\text{NVP}_{11}(2)} + \underbrace{\frac{2L_{12}L_{13}L_{23}s^3}{Z_{11}Z_{22}Z_{33}}}_{\text{NVP}_{11}(3)}; \\
\text{NVP}_{21} &= \underbrace{\frac{L_{12}s}{Z_{22}}}_{\text{NVP}_{21}(1)} + \underbrace{\frac{L_{13}L_{23}s^2}{Z_{22}Z_{33}}}_{\text{NVP}_{21}(2)}; & \text{NVP}_{12} &= \underbrace{\frac{L_{12}s}{Z_{11}}}_{\text{NVP}_{12}(1)} + \underbrace{\frac{L_{12}L_{23}s^2}{Z_{11}Z_{33}}}_{\text{NVP}_{12}(2)}; \\
\text{NVP}_{22} &= -\underbrace{\frac{L_{12}s^2}{Z_{11}Z_{22}}}_{\text{NVP}_{22}(1)} + \underbrace{\frac{L_{23}s^2}{Z_{22}Z_{33}}}_{\text{NVP}_{22}(2)} + \underbrace{\frac{2L_{12}L_{23}L_{13}s^3}{Z_{11}Z_{22}Z_{33}}}_{\text{NVP}_{22}(3)}; \\
\text{NVP}_{13} &= \underbrace{\frac{L_{13}s}{Z_{11}}}_{\text{NVP}_{13}(1)} + \underbrace{\frac{L_{12}L_{23}s^2}{Z_{11}Z_{22}}}_{\text{NVP}_{13}(2)}; & \text{NVP}_{23} &= \underbrace{\frac{L_{23}s}{Z_{22}}}_{\text{NVP}_{23}(1)} + \underbrace{\frac{L_{12}L_{13}s^2}{Z_{11}Z_{22}}}_{\text{NVP}_{23}(2)}; \\
\text{NCP}_{11} &= \underbrace{1}_{\text{NCP}_{11}(1)} + \underbrace{\frac{L_{23}s^2}{Z_{22}Z_{33}}}_{\text{NCP}_{11}(2)}; & \text{NCP}_{21} &= -\underbrace{\frac{L_{12}s}{Z_{11}}}_{\text{NCP}_{21}(1)} + \underbrace{\frac{L_{13}L_{23}s^3}{Z_{11}Z_{33}}}_{\text{NCP}_{21}(2)}; \\
\text{NCP}_{12} &= -\underbrace{\frac{L_{12}s}{Z_{22}}}_{\text{NCP}_{12}(1)} + \underbrace{\frac{L_{13}L_{23}s^2}{Z_{22}Z_{33}}}_{\text{NCP}_{12}(2)}; & \text{NCP}_{22} &= \underbrace{1}_{\text{NCP}_{22}(1)} + \underbrace{\frac{L_{23}s^2}{Z_{11}Z_{33}}}_{\text{NCP}_{22}(2)}; \\
\text{NCP}_{13} &= -\underbrace{\frac{L_{13}s}{Z_{33}}}_{\text{NCP}_{13}(1)} + \underbrace{\frac{L_{12}L_{23}s^2}{Z_{22}Z_{33}}}_{\text{NCP}_{13}(2)}; & \text{NCP}_{23} &= -\underbrace{\frac{L_{23}s}{Z_{33}}}_{\text{NCP}_{23}(1)} + \underbrace{\frac{L_{12}L_{13}s^2}{Z_{11}Z_{33}}}_{\text{NCP}_{23}(2)}; \\
\Delta &= \underbrace{1}_{\Delta(1)} + \underbrace{\frac{L_{13}^2 s^2}{Z_{11}Z_{33}}}_{\Delta(2)} + \underbrace{\frac{L_{23}^2 s^2}{Z_{22}Z_{33}}}_{\Delta(3)} + \underbrace{\frac{L_{12}^2 s^2}{Z_{11}Z_{22}}}_{\Delta(4)} + \underbrace{\frac{2L_{12}L_{23}L_{13}s^3}{Z_{11}Z_{22}Z_{33}}}_{\Delta(5)}
\end{aligned}$$

APPENDIX B

$$\begin{aligned}
\Delta &= \underbrace{1}_{\Delta(1)} - \underbrace{\frac{L_{12}^2 s^2}{Z_{11}Z_{22}}}_{\Delta(2)} - \underbrace{\frac{L_{13}^2 s^2}{Z_{11}Z_{33}}}_{\Delta(3)} - \underbrace{\frac{L_{14}^2 s^2}{Z_{11}Z_{44}}}_{\Delta(4)} - \underbrace{\frac{L_{23}^2 s^2}{Z_{22}Z_{33}}}_{\Delta(5)} - \underbrace{\frac{L_{24}^2 s^2}{Z_{22}Z_{44}}}_{\Delta(6)} - \underbrace{\frac{L_{34}^2 s^2}{Z_{33}Z_{44}}}_{\Delta(7)} \\
&+ \underbrace{\frac{2L_{23}L_{34}L_{24}s^3}{Z_{22}Z_{33}Z_{44}}}_{\Delta(8)} + \underbrace{\frac{2L_{13}L_{34}L_{14}s^3}{Z_{11}Z_{33}Z_{44}}}_{\Delta(9)} + \underbrace{\frac{2L_{12}L_{24}L_{14}s^3}{Z_{11}Z_{22}Z_{44}}}_{\Delta(10)} + \underbrace{\frac{2L_{12}L_{23}L_{13}s^3}{Z_{11}Z_{22}Z_{33}}}_{\Delta(11)} \\
&+ \underbrace{\frac{L_{12}^2 L_{34}^2 s^4}{Z_{11}Z_{22}Z_{33}Z_{44}}}_{\Delta(12)} + \underbrace{\frac{L_{13}^2 L_{24}^2 s^4}{Z_{11}Z_{22}Z_{33}Z_{44}}}_{\Delta(13)} + \underbrace{\frac{L_{14}^2 L_{23}^2 s^4}{Z_{11}Z_{22}Z_{33}Z_{44}}}_{\Delta(14)} + \underbrace{\frac{2L_{12}L_{24}L_{34}L_{13}s^4}{Z_{11}Z_{22}Z_{33}Z_{44}}}_{\Delta(15)} \\
&+ \underbrace{\frac{2L_{12}L_{23}L_{34}L_{14}s^4}{Z_{11}Z_{22}Z_{33}Z_{44}}}_{\Delta(16)} + \underbrace{\frac{2L_{13}L_{23}L_{24}L_{14}s^4}{Z_{11}Z_{22}Z_{33}Z_{44}}}_{\Delta(17)}
\end{aligned}$$

APPENDIX C

$$\begin{aligned}
\text{NVP}_{12} &= \underbrace{\frac{L_{12}s}{Z_{11}}}_{\text{NVP}_{12}(1)} - \underbrace{\frac{L_{12}L_{34}^2 s^3}{Z_{11}Z_{33}Z_{44}}}_{\text{NVP}_{12}(2)} - \underbrace{\frac{L_{13}L_{23}s^2}{Z_{11}Z_{33}}}_{\text{NVP}_{12}(3)} - \underbrace{\frac{L_{14}L_{24}s^2}{Z_{11}Z_{44}}}_{\text{NVP}_{12}(4)} + \underbrace{\frac{L_{13}L_{34}L_{24}s^3}{Z_{11}Z_{33}Z_{44}}}_{\text{NVP}_{12}(5)} \\
&+ \underbrace{\frac{L_{14}L_{23}L_{34}s^3}{Z_{11}Z_{33}Z_{44}}}_{\text{NVP}_{12}(6)}
\end{aligned}$$

APPENDIX D

$$\begin{aligned}
\text{NVP}_{22} &= -\underbrace{\frac{L_{12}^2 s^2}{Z_{11}Z_{22}}}_{\text{NVP}_{22}(1)} - \underbrace{\frac{L_{23}^2 s^2}{Z_{22}Z_{33}}}_{\text{NVP}_{22}(2)} - \underbrace{\frac{L_{24}^2 s^2}{Z_{22}Z_{44}}}_{\text{NVP}_{22}(3)} + \underbrace{\frac{L_{23}L_{34}L_{24}s^3}{Z_{22}Z_{33}Z_{44}}}_{\text{NVP}_{22}(4)} + \underbrace{\frac{L_{12}L_{24}L_{14}s^3}{Z_{11}Z_{22}Z_{44}}}_{\text{NVP}_{22}(5)} \\
&+ \underbrace{\frac{L_{12}L_{23}L_{13}s^3}{Z_{11}Z_{22}Z_{33}}}_{\text{NVP}_{22}(6)} + \underbrace{\frac{L_{12}^2 L_{34}^2 s^4}{Z_{11}Z_{22}Z_{33}Z_{44}}}_{\text{NVP}_{22}(7)} + \underbrace{\frac{L_{14}^2 L_{23}^2 s^4}{Z_{11}Z_{22}Z_{33}Z_{44}}}_{\text{NVP}_{22}(8)} + \underbrace{\frac{L_{13}^2 L_{24}^2 s^4}{Z_{11}Z_{22}Z_{33}Z_{44}}}_{\text{NVP}_{22}(9)} \\
&- \underbrace{\frac{2L_{12}L_{24}L_{34}L_{13}s^4}{Z_{11}Z_{22}Z_{33}Z_{44}}}_{\text{NVP}_{22}(10)} - \underbrace{\frac{2L_{12}L_{23}L_{34}L_{14}s^4}{Z_{11}Z_{22}Z_{33}Z_{44}}}_{\text{NVP}_{22}(11)} - \underbrace{\frac{2L_{14}L_{24}L_{23}L_{13}s^4}{Z_{11}Z_{22}Z_{33}Z_{44}}}_{\text{NVP}_{22}(12)}
\end{aligned}$$

APPENDIX E

$$\begin{aligned}
\text{NCP}_{12} &= -\underbrace{\frac{L_{12}s}{Z_{22}}}_{\text{NCP}_{12}(1)} + \underbrace{\frac{L_{12}L_{34}^2 s^3}{Z_{22}Z_{33}Z_{44}}}_{\text{NCP}_{12}(2)} + \underbrace{\frac{L_{13}L_{23}s^2}{Z_{22}Z_{33}}}_{\text{NCP}_{12}(3)} + \underbrace{\frac{L_{14}L_{24}s^2}{Z_{22}Z_{44}}}_{\text{NCP}_{12}(4)} - \underbrace{\frac{L_{13}L_{34}L_{24}s^3}{Z_{22}Z_{33}Z_{44}}}_{\text{NCP}_{12}(5)} \\
&- \underbrace{\frac{L_{14}L_{23}L_{34}s^3}{Z_{22}Z_{33}Z_{44}}}_{\text{NCP}_{12}(6)}
\end{aligned}$$

APPENDIX F

$$\begin{aligned}
\text{NCP}_{11} &= \underbrace{1}_{\text{NCP}_{11}(1)} - \underbrace{\frac{L_{23}^2 s^2}{Z_{22}Z_{33}}}_{\text{NCP}_{11}(2)} - \underbrace{\frac{L_{24}^2 s^2}{Z_{22}Z_{44}}}_{\text{NCP}_{11}(3)} - \underbrace{\frac{L_{34}^2 s^2}{Z_{33}Z_{44}}}_{\text{NCP}_{11}(4)} + \underbrace{\frac{2L_{23}L_{34}L_{24}s^3}{Z_{22}Z_{33}Z_{44}}}_{\text{NCP}_{11}(5)}
\end{aligned}$$

APPENDIX G

$$\begin{aligned}
Z_{rfl,11}(\text{DM}, \text{AP1}) &= \frac{-L_{12}^2 s^2 Z_{33} - L_{13}^2 s^2 Z_{22} + 2L_{12}L_{23}L_{13}s^3}{Z_{22}Z_{33} - L_{23}^2 s^2}; \\
Z_{rfl,11}(\text{AP2}) &\rightarrow \left(\frac{L_{12}}{L_{23}}\right)^2 Z_{33} - \frac{2L_{12}L_{13}}{L_{23}} s; & Z_{rfl,11}(\text{AP3}) &\rightarrow \left(\frac{L_{12}}{L_{23}}\right)^2 Z_{33}; \\
Z_{rfl,22}(\text{DM}) &= \frac{-L_{12}^2 s^2 Z_{33} - L_{23}^2 s^2 Z_{11} + 2L_{12}L_{23}L_{13}s^3}{Z_{11}Z_{33} - L_{13}^2 s^2}; \\
Z_{rfl,22}(\text{AP1}, \text{AP2}) &\rightarrow -\frac{L_{23}^2 s^2}{Z_{33}}; & Z_{rfl,22}(\text{AP3}) &= -\frac{L_{23}^2 s^2}{Z_{33}} - \frac{L_{12}^2 s^2}{Z_{11}}; \\
Z_{rfl,33}(\text{DM}) &= \frac{-L_{13}^2 s^2 Z_{22} - L_{23}^2 s^2 Z_{11} + 2L_{12}L_{23}L_{13}s^3}{Z_{11}Z_{22} - L_{12}^2 s^2}; \\
Z_{rfl,33}(\text{AP1}, \text{AP3}) &\rightarrow -\frac{L_{23}^2 s^2}{Z_{22}}; & Z_{rfl,33}(\text{AP2}) &\rightarrow \infty;
\end{aligned}$$

REFERENCES

- [1] H. Vázquez-Leal, A. Gallardo-Del-Angel, R. Castañeda-Sheissa, and F. J. González-Martínez, "The phenomenon of wireless energy transfer: Experiments and philosophy," in *Wireless Power Transfer*, K. Y. Kim, Ed. Rijeka: IntechOpen, 2012, ch. 1. [Online]. Available: <https://doi.org/10.5772/25829>
- [2] S. Li and C. C. Mi, "Wireless power transfer for electric vehicle applications," *IEEE Journal of Emerging and Selected Topics in Power Electronics*, vol. 3, no. 1, pp. 4–17, March 2015.
- [3] C. T. Rim and C. Mi, *Introduction to Dynamic Charging*. John Wiley & Sons, Ltd, 2017, ch. 8, pp. 155–160. [Online]. Available: <https://onlinelibrary.wiley.com/doi/abs/10.1002/9781119329084.ch8>
- [4] M. Budhia, J. T. Boys, G. A. Covic, and C. Huang, "Development of a single-sided flux magnetic coupler for electric vehicle IPT charging systems," *IEEE Transactions on Industrial Electronics*, vol. 60, no. 1, pp. 318–328, Jan 2013.
- [5] A. K. RamRakhyani, S. Mirabbasi, and M. Chiao, "Design and optimization of resonance-based efficient wireless power delivery systems for biomedical implants," *IEEE Transactions on Biomedical Circuits and Systems*, vol. 5, no. 1, pp. 48–63, Feb 2011.
- [6] A. P. Sample, D. T. Meyer, and J. R. Smith, "Analysis, experimental results, and range adaptation of magnetically coupled resonators for wireless power transfer," *IEEE Transactions on Industrial Electronics*, vol. 58, no. 2, pp. 544–554, Feb 2011.
- [7] N. Suh and D. Cho, *The on-line electric vehicle: Wireless electric ground transportation systems*, 04 2017.
- [8] A. Kurs, A. Karalis, R. Moffatt, J. D. Joannopoulos, P. Fisher, and M. Soljačić, "Wireless power transfer via strongly coupled magnetic resonances," *Science*, vol. 317, no. 5834, pp. 83–86, 2007. [Online]. Available: <https://science.sciencemag.org/content/317/5834/83>
- [9] W. X. Zhong, C. K. Lee, and S. Y. Hui, "Wireless power domino-resonator systems with noncoaxial axes and circular structures," *IEEE Transactions on Power Electronics*, vol. 27, no. 11, pp. 4750–4762, Nov 2012.
- [10] J. Kim, H. Son, D. Kim, and Y. Park, "Optimal design of a wireless power transfer system with multiple self-resonators for an LED TV," *IEEE Transactions on Consumer Electronics*, vol. 58, no. 3, pp. 775–780, August 2012.
- [11] S. Zhou and C. Chris Mi, "Multi-paralleled LCC reactive power compensation networks and their tuning method for electric vehicle dynamic wireless charging," *IEEE Transactions on Industrial Electronics*, vol. 63, no. 10, pp. 6546–6556, Oct 2016.
- [12] F. Lu, H. Zhang, H. Hofmann, and C. C. Mi, "A dynamic charging system with reduced output power pulsation for electric vehicles," *IEEE Transactions on Industrial Electronics*, vol. 63, no. 10, pp. 6580–6590, Oct 2016.
- [13] A. Zaheer, H. Hao, G. A. Covic, and D. Kacprzak, "Investigation of multiple decoupled coil primary pad topologies in lumped IPT systems for interoperable electric vehicle charging," *IEEE Transactions on Power Electronics*, vol. 30, no. 4, pp. 1937–1955, April 2015.
- [14] F. Faradjizadeh, M. Vilathgamuwa, D. Jovanovic, P. Jayathurathnage, G. Ledwich, and U. Madawala, "Expandable n-legged converter to drive closely spaced multi transmitter wireless power transfer systems for dynamic charging," *IEEE Transactions on Power Electronics*, pp. 1–1, 2019.
- [15] B. Lee and D. Ahn, "Robust self-regulated rectifier for parallel-resonant Rx coil in multiple-receiver wireless power transmission system," *IEEE Journal of Emerging and Selected Topics in Power Electronics*, pp. 1–1, 2019.
- [16] Z. Pantic, S. Bai, and S. M. Lukic, "ZCS LCC-compensated resonant inverter for inductive-power-transfer application," *IEEE Transactions on Industrial Electronics*, vol. 58, no. 8, pp. 3500–3510, Aug 2011.
- [17] K. Song, Z. Li, J. Jiang, and C. Zhu, "Constant current/voltage charging operation for series-series and series-parallel compensated wireless power transfer systems employing primary-side controller," *IEEE Transactions on Power Electronics*, vol. 33, no. 9, pp. 8065–8080, Sep. 2018.
- [18] Y. Yang, W. Zhong, S. Kiratipongvoot, S. Tan, and S. Y. R. Hui, "Dynamic improvement of series-series compensated wireless power transfer systems using discrete sliding mode control," *IEEE Transactions on Power Electronics*, vol. 33, no. 7, pp. 6351–6360, July 2018.
- [19] A. Pacini, A. Costanzo, S. Aldhaher, and P. D. Mitcheson, "Load- and position-independent moving MHz wpt system based on GaN-distributed current sources," *IEEE Transactions on Microwave Theory and Techniques*, vol. 65, no. 12, pp. 5367–5376, Dec 2017.
- [20] C. Rong, C. Lu, Z. Hu, X. Huang, X. Tao, S. Wang, B. Wei, S. Wang, and M. Liu, "Analysis of wireless power transfer based on metamaterial using equivalent circuit," *The Journal of Engineering*, vol. 2019, no. 16, pp. 2032–2035, 2019.
- [21] Y. Fang and M. H. Pong, "A bayesian optimization and partial element equivalent circuit approach to coil design in inductive power transfer systems," in *2018 IEEE PELS Workshop on Emerging Technologies: Wireless Power Transfer (Wow)*, June 2018, pp. 1–5.
- [22] J. C. Coetzee and Y. Liu, "Compact multiport antenna with isolated ports," in *2008 IEEE International RF and Microwave Conference*, Dec 2008, pp. 229–232, 2008. [Online]. Available: <https://onlinelibrary.wiley.com/doi/abs/10.1002/mop.23038>
- [23] J. C. Coetzee and Y. Yu, "A compact monopole array with decoupled ports," in *2008 IEEE International RF and Microwave Conference*, Dec 2008, pp. 112–116.
- [24] C. K. Lee, W. X. Zhong, and S. Y. R. Hui, "Effects of magnetic coupling of nonadjacent resonators on wireless power domino-resonator systems," *IEEE Transactions on Power Electronics*, vol. 27, no. 4, pp. 1905–1916, April 2012.
- [25] S. J. Mason, "Feedback theory-further properties of signal flow graphs," *Proceedings of the IRE*, vol. 44, no. 7, pp. 920–926, July 1956.
- [26] W. K. Chen and C. Satyanarayana, "Applied graph theory: Graphs and electrical networks," *IEEE Transactions on Systems, Man, and Cybernetics*, vol. 8, no. 5, pp. 418–418, May 1978.
- [27] L. Robichaud, M. Boisvert, and J. Robert, *Signal Flow Graphs and Applications*, ser. Prentice-Hall electrical engineering series. Prentice-Hall, 1962. [Online]. Available: <https://books.google.com.au/books?id=6Q0jAAAAAMAAJ>
- [28] B. Bollobás, B. s, S. Axler, B. Bollobas, F. Gehring, S. S. Media, and P. Halmos, *Modern Graph Theory*, ser. Graduate Texts in Mathematics. Springer New York, 1998. [Online]. Available: <https://books.google.com.au/books?id=SbZKSZ-1qrwC>
- [29] J. Hou, Q. Chen, Z. Zhang, S. Wong, and C. K. Tse, "Analysis of output current characteristics for higher order primary compensation in inductive power transfer systems," *IEEE Transactions on Power Electronics*, vol. 33, no. 8, pp. 6807–6821, Aug 2018.
- [30] W. Zhang and C. C. Mi, "Compensation topologies of high-power wireless power transfer systems," *IEEE Transactions on Vehicular Technology*, vol. 65, no. 6, pp. 4768–4778, June 2016.
- [31] N. A. Keeling, G. A. Covic, and J. T. Boys, "A unity-power-factor IPT pickup for high-power applications," *IEEE Transactions on Industrial Electronics*, vol. 57, no. 2, pp. 744–751, Feb 2010.



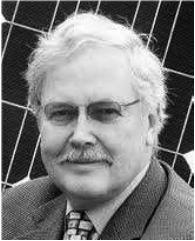
Farzad Farajizadeh (Farajizadeh) (S'14) received the B.S. degree in electrical engineering from the Azad University of Gonabad, Iran, in 2009, and the M.S. degree in electrical engineering from the Azad University of Tehran, Tehran, Iran, in 2010. He is currently working toward the Ph.D. degree at Queensland University of Technology, Brisbane, Qld., Australia. His current research interests include wireless power transfer systems, power electronic converters, machine drives, FACTS, and renewable energy conversion.



D. Mahinda Vilathgamuwa (S'90–M'93– SM'99) received the B.Sc. degree in electrical engineering from the University of Moratuwa, Sri Lanka, in 1985, and the Ph.D. degree in electrical engineering from Cambridge University, U.K., in 1993. He joined the School of Electrical and Electronic Engineering, Nanyang Technological University, Singapore, in 1993. He is currently a Professor of power engineering with the Queensland University of Technology, Brisbane, QLD, Australia. He has published over 300 research papers in refereed journals and conferences. His research interests include wireless power, power electronic converters, battery storage, and electromobility. He is an associate editor of *IEEE Transactions on Industrial Electronics*.



Prasad Jayathurathnage (S'12-M'17) received the B.Sc. degree in electronics and telecommunications engineering from the University of Moratuwa, Sri Lanka, in 2009, and the Ph.D. degree in the School of Electrical and Electronic Engineering, Nanyang Technological University, Singapore, in 2017. He is currently a Postdoctoral Researcher with the Aalto University, Finland. His research interests include high-frequency power converters, wireless power transfer, and biomedical implants.



Gerard Ledwich (SM'89) received the Ph.D. degree in electrical engineering from the University of New-castle, Newcastle, NSW, Australia, in 1976. He is a research Professor of electric power with the School of Electrical Engineering and Computer Science, Queensland University of Technology, Brisbane, QLD, Australia. His research interests include power systems, power electronics, and wide area control of smart grid.